

On the environments of type Ia supernovae within host galaxies

J. P. Anderson^{1*}, P. A. James², F. Förster^{3,4}, S. González-Gaitán^{3,5},
S. M. Haberman², M. Hamuy^{5,3}, J. D. Lyman⁶

¹European Southern Observatory, Alonso de Cordova 3107, Vitacura, Casilla 19001, Santiago, Chile

²Astrophysics Research Institute, Liverpool John Moores University, IC2, Liverpool Science Park, 146 Brownlow Hill, Liverpool, L3 5RF, UK

³Millennium Institute of Astrophysics, Santiago, Chile

⁴Center for Mathematical Modelling, Universidad de Chile, Avenida Blanco Encalada 2120 Piso 7, Santiago, Chile

⁵Departamento de Astronomía, Universidad de Chile, Casilla 36-D, Santiago, Chile

⁶Department of Physics, University of Warwick, Coventry, CV4 7AL, UK

ABSTRACT

We present constraints on supernovae type Ia (SNe Ia) progenitors through an analysis of the environments found at the explosion sites of 102 events within star-forming host galaxies. $H\alpha$ and *GALEX* near-UV images are used to trace on-going and recent star formation (SF), while broad band *B*, *R*, *J*, *K* imaging is also analysed. Using pixel statistics we find that SNe Ia show the lowest degree of association with $H\alpha$ emission of all supernova types. It is also found that they do not trace near-UV emission. As the latter traces SF on timescales less than 100 Myr, this rules out any extreme ‘prompt’ delay-times as the dominant progenitor channel of SNe Ia. SNe Ia best trace the *B*-band light distribution of their host galaxies. This implies that the population within star-forming galaxies is dominated by relatively young progenitors. Splitting SNe by their (*B*-*V*) colours at maximum light, ‘redder’ events show a higher degree of association to H II regions and are found more centrally within hosts. We discuss possible explanations of this result in terms of line of sight extinction and progenitor effects. No evidence for correlations between SN stretch and environment properties is observed.

Key words: supernovae: general, galaxies: statistics

1 INTRODUCTION

Type Ia supernovae (SNe Ia henceforth) are considered to arise from the accretion of matter onto a white dwarf (WD) star in a binary system. This process is thought to increase the WD mass to the point where ignition leads to a runaway thermonuclear explosion of the WD system (see Wang & Han 2012 and Maoz et al. 2014 for recent reviews). Indeed, for the very nearby SN Ia SN 2011fe, the primary progenitor star was directly constrained to be a compact degenerate object for the first time (Nugent et al. 2011; Bloom et al. 2012, also see SN 2013dy, Zheng et al. 2013). However, many processes remain poorly constrained meaning that we still have little idea on the exact explosion physics or the progenitor parameter space that permits a successful explosion. These issues are particularly pertinent given the use of SNe Ia in many areas of astrophysics. SNe Ia have been used as accurate distance indicators, which led to the discovery of the accelerated expansion of the Universe (Riess et al. 1998; Perlmutter et al. 1999). In addition, SNe Ia are the main producers of iron peak elements in the Universe and hence are particularly important for understanding chemical evolution processes (see e.g. Matteucci et al. 2006;

Kobayashi & Nomoto 2009 and references therein).

While the exact details of the progenitor systems remain unclear, the two most popular are the single degenerate (SD), and double degenerate (DD) scenarios. In the SD scenario (e.g. Whelan & Iben 1973), a WD accretes matter from a companion MS or RG star, increasing its mass towards the Chandrasekhar mass, which leads to carbon ignition and ensuing explosion. In the DD scenario (e.g. Iben & Tutukov 1984), a double WD system loses angular momentum due to gravitational wave emission, leading to coalescence and explosion. There also exist scenarios where the WD ignites and explodes at masses both below (e.g. Nomoto 1982) and above (e.g. Hachisu et al. 2012, Pakmor et al. 2012 and references therein) the Chandrasekhar mass. Indeed, Scalzo et al. (2014) showed that a significant fraction of ‘normal’ SNe Ia explode with significantly sub-Chandrasekhar ejecta masses. Various lines of evidence have been presented, much coming in recent years, however a preference for one specific progenitor system for the majority of SNe Ia events is still lacking.

The initial classification of SNe into massive stars which core-collapse (CC SNe), and lower mass progenitor systems which lead to thermonuclear explosions was given credence by the observation that CC SNe (SNe II and SNe Ibc) are exclusively observed to occur in star-forming galaxies, while SNe Ia are found to ex-

* E-mail: janderso@eso.org

plode in all galaxy types (e.g. van den Bergh et al. 2002). Given that elliptical galaxies are dominated by old stellar populations, this constrains at least a fraction of the progenitors of SNe Ia to be similarly evolved systems. More involved studies have investigated how the SN Ia rate changes with redshift together with host galaxy properties such as colour, mass, star formation rate (SFR), and specific SFR (sSFR) (e.g. Strolger et al. 2004; Mannucci et al. 2005; Förster et al. 2006; Sullivan et al. 2006). These results have been used to constrain the delay time distribution (DTD) of SNe Ia (distribution of times between epoch of star formation, SF, and explosion), with claims of ‘prompt’ and ‘tardy’ components (see e.g. Scannapieco & Bildsten 2005; Mannucci et al. 2006). Indeed the SN Ia rate is consistent with the ‘prompt’ component being proportional to the SFR, and the ‘tardy’ component being consistent with stellar mass of host galaxies (see e.g. Sullivan et al. 2006, and more recently Smith et al. 2012). DTDs have also been derived using the star formation history (SFH) of galaxies within a given SN search program (Maoz et al. 2011, 2012).

The defining characteristic that has allowed SNe Ia to be used as distance indicators, is their low intrinsic peak luminosity dispersion (~ 0.35 mag, Branch & Miller 1993). This dispersion is lowered further once correlations between luminosities and both SN decline rates and intrinsic colours are adopted (Phillips 1993; Hamuy et al. 1996a; Riess et al. 1996). Investigations have proceeded to find correlations between light-curve parameters and host galaxy properties. Hamuy et al. (2000) (following Hamuy et al. 1996b) found that brighter SNe Ia are preferentially found within younger stellar populations. These initial results have been confirmed (see e.g. Johansson et al. 2013) and further investigated, with indications that brighter events also prefer lower metallicity galaxies (Gallagher et al. 2008; Howell et al. 2009; Neill et al. 2009). These differences would only be important for cosmological studies if correlations remained *after* SN luminosities had been corrected for light-curve properties. Numerous recent studies have concentrated on searching for such correlations with Hubble residuals. Indeed, evidence has now been presented from multiple independent investigators that Hubble residuals show correlations with host galaxy properties, in particular galaxy mass (Kelly et al. 2010; Sullivan et al. 2010; Lampeitl et al. 2010; Gupta et al. 2011; D’Andrea et al. 2011; Johansson et al. 2013; Hayden et al. 2013; Childress et al. 2013; Pan et al. 2014). This could have important consequences for the continued use of SNe Ia as accurate distance indicators out to higher redshifts, if these effects are not properly accounted for. While determining whether stellar population age or metallicity is the driving factor behind these correlations is somewhat difficult, several studies have strongly argued that progenitor age is the dominant parameter, with lower mass, higher sSFR galaxies producing younger SN Ia explosions (Childress et al. 2013; Johansson et al. 2013; Rigault et al. 2013).

While many large samples of global SN Ia host galaxy property studies have now been published, studies of the environments of SNe Ia *within* host galaxies, such as those now regularly seen for CC SNe (see e.g. Modjaz et al. 2008; Kelly & Kirshner 2012; Anderson et al. 2012 and references therein), are, to-date rare in the literature. The obvious reason for this is the significantly older progenitor populations of SNe Ia –and the therefore increased delay between SF and explosion– implies that the majority of SNe Ia will explode far from their birth places. This could then restrict the relevance of information that can be extracted from such studies. However, some work in this direction does exist.

The first approach involved investigating the radial distribution of SNe, to see whether different SNe Ia preferentially occur at

specific radial positions within galaxies. Given that stellar population properties such as age, extinction, and metallicity change with radial positions, one can associate SN properties to those of the stellar populations found at those same regions. Wang et al. (1997) first suggested that there is a deficit of SN Ia in the central parts of galaxies, which was not observed for CC SNe. Ivanov et al. (2000) correlated SN properties with galactocentric radii and found that the range in brightness and light-curve width of SNe Ia increased with increasing radial distance from the centres of host galaxies, suggesting this was a progenitor age effect. Förster & Schawinski (2008) analysed the radial distribution of SN Ia in elliptical galaxies, finding that there was no statistical difference between the radial distribution of SN Ia and the light profile of their hosts. They concluded that this implied that some SN Ia progenitors do have delay times of several Gyr. More recently, Galbany et al. (2012) found that the average SN extinction and colour was correlated with radial position. Wang et al. (2013) have claimed that two distinct populations of SNe Ia exist, apparently implied from differences in the ejecta velocities of SNe found within the inner and outer regions of host galaxies. However, recently Pan et al. (2015) presented a separate analysis where the same trend was observed but with less significance.

To further investigate the local environments of SNe, one can analyse the properties of the stellar populations at the exact site of SNe. Kelly et al. (2008) employed pixel statistics (in a very similar fashion to that which we will use in the current analysis) finding that the SNe Ia population statistically followed the distribution of g' -band light of their hosts, in a similar fashion to SNe II. Comparing those statistics to an analytical model of spiral galaxy light distributions, Raskin et al. (2009) concluded that even the most ‘prompt’ SNe Ia have delay times of more than a few 100 Myrs. Wang et al. (2013) found that SNe Ia with higher ejecta velocities fall on brighter regions of their hosts than those with lower measured velocities. In addition, Rigault et al. (2013) showed that SNe Ia occurring in regions with detected $H\alpha$ emission are ‘redder’ than those exploding where no emission is found. Meanwhile, Galbany et al. (2014) published a study of SNe environments using integral field spectroscopy (IFS). They showed through a variety of indicators that SNe Ia were found to occur further from star-forming regions than CC SNe. In addition they found that the SNe Ia location properties were on average the same as those measured globally. It is clear that future IFS studies will be particularly revealing for SN environment analyses. Most recently Kelly et al. (2014) demonstrated that SN Ia falling on regions of high UV surface brightness and SF density, appear to show significantly lower Hubble residuals, hence improving the accuracy of a sub-set of SN Ia as distance indicators. This result was actually predicted in Childress et al. (2014) who suggested that SN Ia selected exclusively from star-forming host galaxies would yield a more cosmologically uniform sample.

In summary, SN environment analyses to-date have shown some intriguing results, which despite the significant delay times of their progenitors, demonstrate that these types of studies can indeed be revealing for SNe Ia. As expected, SNe Ia explode in distinct environments to CC SNe (see e.g. initial study in James & Anderson 2006), confirming their older progenitors. There appears to be a deficit of SNe in the central regions of star-forming galaxies, which perhaps implies that the old bulge populations of these galaxies are not significant producers of SNe Ia. Meanwhile, environment studies suggest that at least a significant fraction of SN Ia colour diversity is produced by host galaxy extinction, due to the preference of ‘redder’ SNe for more central regions and for higher $H\alpha$

flux environments. There is also an intriguing suggestion that environments can be used to select SNe samples with lower Hubble residuals. However, the above also shows that environment studies are still somewhat in their infancy, particularly when compared to studies of light-curve properties. Investigations have generally concentrated on one specific measurement, and often suffer from insufficient statistics. Hence, a more wide ranging study of SN Ia environments, which attempts to bring together many of the aspects of the above is warranted.

In the current paper we further investigate the properties of the immediate environments of SNe Ia within star-forming host galaxies, using multi-colour host galaxy pixel statistics, and the radial distribution of events with respect to both SF and the older stellar continuum population. This follows from James & Anderson (2006) where a small sample of SNe Ia were analysed using these techniques.

The paper is organised as follows. In the next section we discuss the SN and galaxy samples, and summarise how we obtained our data and their reduction. In § 3 the statistical methods we employ are discussed, and in § 4 the results are presented. This is followed by a discussion of their implications for our understanding of SNe Ia transient and progenitor properties in § 5. Finally we summarise and list our main conclusions in § 6.

2 SUPERNOVA AND HOST GALAXY SAMPLES

The sample we study is a compilation of SNe and their host galaxies from the literature. Initially, the sample was formed from SNe which had occurred within the H α Galaxy Survey (H α GS; James et al. 2004), a representative survey of star-forming galaxies within the local Universe. Since the analysis of those data (James & Anderson 2006), a significantly larger sample of H α and R - or r' -band host galaxy observations have been obtained. The only criterion for obtaining these data was that a) host galaxies had recession velocities less than 6000kms^{-1} so that we can probe distinct stellar populations¹, b) that host galaxies had major to minor axis ratios of less than 4:1 to reduce issues with chance superpositions of foreground or background stellar populations onto SNe explosion sites, and c) hosts were targeted where individual SNe had published photometry, so that light-curve parameters could be derived and compared to environmental information. Our initial aim to investigate the association of SNe Ia with SF within galaxies restricts our sample to star-forming late-type galaxies. Later we will analyse and discuss possible systematics that this may bring to our conclusions. The sample of SNe and their host galaxies is listed in Table 1, together with derived SN light-curve parameters. Before describing host galaxy observations, we outline the methods for extracting light-curve parameters for our sample using literature photometry.

2.1 Light-curve parameters

In addition to analysing the environments of SNe Ia as an overall population, it is also fruitful to analyse whether specific SN Ia properties show correlations with their environment. This is motivated by differences in SNe light-curve parameters found with

global galaxy properties. Observables of individual SNe Ia can be extracted from their optical light-curves. To proceed, literature photometric data was searched for all SNe in our sample. Where useful photometry was found we list the source in Table 1. We then use *SIFTO* (Conley et al. 2008), a light-curve fitter that uses spectral template time series that are adjusted to the observed colours of SN Ia photometry to obtain values of B -band maximum date, a light-curve width parameter or ‘stretch’ of the time-axis relative to the template, and multiplicative factors for each band from which an observed $(B-V)_{max}$ colour is obtained. In order to include photometry in our analysis we require that for colour estimations at least one photometric point is available between -15 and $+8$ days, and one available between $+5$ and $+25$ days with respect to B -band maximum in both the B and V bands. In the case of stretch we include SNe if data is available in only one of these bands (or other filters). Furthermore, we only include light-curve fits which give stretch values in the range 0.4 – 1.6 . Redshift and Galactic extinction are additional inputs to the fitter. The fitted colour is a combination of intrinsic colour and host reddening, for which no extinction law is applied. We recall that stretch is highly correlated with SN brightness, with higher stretch events being intrinsically brighter SNe (Perlmutter et al. 1997). The resulting light-curve parameters are listed in Table 1.²

2.2 Host galaxy observations

The principal aim of this work is to analyse the association of SNe Ia with SF within their host galaxies. To proceed with this aim we use our own H α imaging, plus *GALEX* near-UV imaging taken from the *GALEX* database³. The original H α imaging galaxy sample was taken from the H α GS survey. Additional data has since been obtained through various time allocations, and the sample we present here is of H α plus R - or r' -band (henceforth we will refer to both of these as simply ‘ R -band’) imaging of 102 SN Ia host galaxies. In addition to H α and near-UV imaging which we use to trace SF on differing time scales, we also analyse host environment properties using R -band imaging together with B -band, plus J - and K -band near-IR images. Next each dataset which forms our sample is discussed in detail, documenting how they were obtained, their reduction, and finally what type of information can be gained by analysing host galaxy imaging at those specific wavebands.

2.3 Host galaxy H α and R -band imaging

H α line emission within galaxies traces regions of young ongoing SF. The emission is produced from the recombination of interstellar medium (ISM) hydrogen atoms after ionisation from the intense UV flux of young massive stars. The massive stars which make the dominant contribution to this ionising flux are of >15 – $20 M_{\odot}$, and therefore H II regions within galaxies are thought to trace SF of ages of less than ~ 10 Myrs (Kennicutt 1998). This is obviously much younger than even the most ‘prompt’ SN Ia scenarios (Aubourg et al. 2008). However, it will be shown that an

² While it would seem interesting to correlate environmental information with Hubble residuals, once we make a redshift cut to the SNe with light-curve information (to remove the effect of galaxy peculiar velocities) the resulting sample is too small to apply such statistical tests as outlined here.

³ <http://archive.stsci.edu/index.html>

¹ A couple of slightly higher recession velocity host galaxies are included, but make no difference to the overall results presented in the paper.

Table 1. SN and host galaxy parameters

| SN | Host galaxy | Galaxy type | V_r (kms $^{-1}$) | Stretch | $(B-V)_{max}$ | Photometry references |
|--------------------|---------------|-----------------|----------------------|---------|---------------|--|
| 1937C | IC 4182 | SAm | 321 | 1.227 | ... | Pierce & Jacoby (1995) |
| 1954B | NGC 5668 | SAd | 1577 | ... | ... | ... |
| 1957A | NGC 2841 | SAb | 638 | ... | ... | ... |
| 1963I | NGC 4178 | SBdm | 374 | ... | ... | ... |
| 1963J | NGC 3913 | SAd | 954 | ... | ... | ... |
| 1968E | NGC 2713 | SBab | 3922 | ... | ... | ... |
| 1968I | NGC 4981 | SABbc | 1680 | ... | ... | ... |
| 1969C | NGC 3811 | SBcd | 3105 | ... | ... | ... |
| 1971G ⁴ | NGC 4165 | SABa | 1859 | ... | ... | ... |
| 1972H ⁵ | NGC 3147 | SAbc | 2802 | ... | ... | ... |
| 1974G | NGC 4414 | SAc | 716 | ... | ... | ... |
| 1975A | NGC 2207 | SABbc | 2741 | ... | ... | ... |
| 1979B | NGC 3913 | SAd | 954 | ... | ... | ... |
| 1981B | NGC 4536 | SABbc | 1808 | ... | ... | ... |
| 1982B | NGC 2268 | SABbc | 2222 | ... | ... | ... |
| 1983U | NGC 3227 | SAB | 1157 | ... | ... | ... |
| 1986A | NGC 3367 | Sbc | 3040 | ... | ... | ... |
| 1986G | NGC 5128 | S0 ⁶ | 547 | 0.717 | 0.839 | Phillips et al. (1987) |
| 1987D | MCG +00-32-01 | SBbc | 2217 | ... | ... | ... |
| 1987O | MCG +02-20-09 | S | 4678 | ... | ... | ... |
| 1989A | NGC 3687 | SABbc | 2507 | ... | ... | ... |
| 1989B | NGC 3627 | SABb | 727 | 0.940 | 0.394 | Wells et al. (1994) |
| 1990N | NGC 4639 | SABbc | 1018 | 1.064 | 0.041 | Lira et al. (1998) |
| 1991T | NGC 4527 | SABbc | 1736 | 1.068 | 0.082 | Ford et al. (1993); Lira et al. (1998) Altavilla et al. (2004) |
| 1991ak | NGC 5378 | SBa | 3042 | ... | ... | ... |
| 1992G | NGC 3294 | SAc | 1586 | ... | ... | ... |
| 1992K | ESO 269-G57 | SABb | 3106 | ... | ... | ... |
| 1992bc | ESO 300-G09 | Sab | 5996 | 1.059 | -0.089 | Hamuy et al. (1996) |
| 1994S | NGC 4495 | Sab | 4550 | 1.030 | -0.021 | Riess et al. (1999) |
| 1994ae | NGC 3370 | SAc | 1279 | 1.054 | -0.050 | Altavilla et al. (2004); Riess et al. (2005) |
| 1995D | NGC 2962 | SAB0 | 1966 | 1.089 | 0.033 | Patat et al. (1996); Meikle et al. (1996) Altavilla et al. (2004) |
| 1995E | NGC 2441 | SABb | 3470 | 0.958 | 0.679 | Riess et al. (1999) |
| 1995al | NGC 3021 | SAbc | 1541 | 1.074 | 0.107 | Riess et al. (1999) |
| 1996Z | NGC 2935 | SABb | 2271 | 0.915 | ... | Riess et al. (1999) |
| 1996ai | NGC 5005 | SABbc | 946 | 1.097 | 1.553 | Riess et al. (1999) |
| 1997Y | NGC 4675 | SBb | 4757 | ... | ... | ... |
| 1997bp | NGC 4680 | Pec | 2492 | 1.016 | 0.152 | Jha et al. (2006) |
| 1997bq | NGC 3147 | SAbc | 2802 | 0.917 | 0.031 | Jha et al. (2006) |
| 1997do | UGC 3845 | SBbc | 3034 | 0.975 | 0.018 | Jha et al. (2006) |
| 1997dt | NGC 7448 | SAbc | 2194 | ... | ... | ... |
| 1998D | NGC 5440 | Sa | 3689 | 0.869 | -0.046 | Jha et al. (2006) |
| 1998aq | NGC 3982 | SABb | 1109 | 0.986 | -0.104 | Riess et al. (2005) |
| 1998bu | NGC 3368 | SABab | 897 | 0.974 | 0.269 | Suntzeff et al. (1999) |
| 1998dh | NGC 7541 | SBbc | 2689 | 0.939 | 0.088 | Jha et al. (2006); Ganeshalingam et al. (2010) |
| 1998eb | NGC 1961 | SABc | 3934 | ... | ... | ... |

investigation into the association of SNe Ia with these regions can still produce interesting results.

The narrow band $H\alpha$ imaging technique involves observing through a narrow $H\alpha$ filter (on the order of 50-100 Å) together with separate broad-band imaging to remove the continuum. Here, we use R or r' filters to remove this component. This also allows us to use these images for further analysis. The initial data used for this project (imaging from $H\alpha$ GS, James et al. 2004) were obtained with the 1.0 metre Jacobus Kapteyn Telescope (JKT), with a pixel scale of 0.333'' per pixel. In the first paper of the current series (James & Anderson 2006), data and analysis were published for 12 SN Ia host environments. Here we significantly increase this

sample size. $H\alpha$ and R -band imaging data were obtained with the Wide Field Camera (0.333'' per pixel image scale) mounted on the Isaac Newton Telescope (INT) over the course of two observing runs during February of both 2007 and 2008. In addition, we searched through a series of previous INT data samples taken for other projects by co-authors of the current paper for further host galaxy imaging. During various time allocations between 2005 and 2009 host galaxy $H\alpha$ and r' band imaging was obtained with RATCAM on the Liverpool Telescope (LT, Steele et al. 2004), with a pixel scale of 0.278'' per pixel. Most recently $H\alpha$ and R -band data were obtained with the MPG/ESO 2.2m telescope together with the Wide Field Imager (WFI, Baade et al. 1999)

Table 1. *Continued...*

| SN | Host galaxy | Galaxy type | V_r (kms $^{-1}$) | Stretch | $(B-V)_{max}$ | Photometry references |
|--------|---------------|------------------|----------------------|---------|---------------|---|
| 1999aa | NGC 2595 | SABc | 4330 | 1.113 | -0.036 | Altavilla et al. (2004); Jha et al. (2006) |
| 1999bh | NGC 3435 | Sb | 5158 | 0.818 | 0.872 | Ganeshalingam et al. (2010) |
| 1999bv | MCG +10-25-14 | S | 5595 | ... | ... | ... |
| 1999by | NGC 2841 | SAb | 638 | 0.618 | 0.484 | Garnavich et al. (2004); Ganeshalingam et al. (2010) |
| 1999cl | NGC 4501 | SAb | 2281 | 0.939 | 1.059 | Krisciunas et al. (2006); Jha et al. (2006) Ganeshalingam et al. (2010) |
| 1999cp | NGC 5468 | SABcd | 2842 | 0.994 | -0.027 | Krisciunas et al. (2000); Ganeshalingam et al. (2010) |
| 1999gd | NGC 2623 | Pec | 5549 | 0.976 | 0.367 | Jha et al. (2006) |
| 2000E | NGC 6951 | SABbc | 1424 | 1.052 | 0.130 | Valentini et al. (2003); Tsvetkov (2006) Lair et al. (2006) |
| 2000ce | UGC 4195 | SBb | 4888 | ... | ... | ... |
| 2001E | NGC 3905 | SBc | 5774 | 1.002 | -0.023 | Ganeshalingam et al. (2010) |
| 2001ay | IC 4423 | S | 9067 | 1.600 | ... | Hicken et al. (2009) |
| 2001bg | NGC 2608 | SBb | 2135 | 0.935 | 0.171 | Ganeshalingam et al. (2010) |
| 2001cz | NGC 4679 | SAbc | 4643 | 1.006 | 0.090 | Krisciunas et al. (2004) |
| 2001eg | UGC 3885 | S | 3809 | ... | ... | ... |
| 2002au | UGC 5100 | SBb | 5514 | ... | ... | ... |
| 2002bs | IC 4221 | SAc | 2889 | ... | ... | ... |
| 2002cr | NGC 5468 | SABcd | 2842 | 0.945 | -0.013 | Hicken et al. (2009) |
| 2002er | UGC 10743 | Sa | 2569 | 0.930 | 0.138 | Pignata et al. (2004); Ganeshalingam et al. (2010) |
| 2002fk | NGC 1309 | SAbc | 2136 | 1.010 | -0.093 | Hicken et al. (2009) |
| 2003cg | NGC 3169 | SAa | 1238 | 0.984 | 1.110 | Elias-Rosa et al. (2006); Hicken et al. (2009) Ganeshalingam et al. (2010) |
| 2003cp | MCG +10-12-78 | Sb | 5927 | ... | ... | ... |
| 2003du | UGC 9391 | SBdm | 1914 | 1.019 | -0.084 | Leonard et al. (2005) |
| 2004bc | NGC 3465 | Sab | 7221 | ... | ... | ... |
| 2004bd | NGC 3786 | SABa | 2678 | ... | ... | ... |
| 2005A | NGC 958 | SBc | 5738 | 0.977 | 0.986 | Contreras et al. (2010) |
| 2005F | MCG +02-23-27 | S | 8545 | ... | ... | ... |
| 2005G | UGC 8690 | Scd | 6938 | ... | ... | ... |
| 2005M | NGC 2930 | S | 7382 | 1.114 | 0.312 | Stritzinger et al. (2011) |
| 2005W | NGC 691 | SAbc | 2665 | 0.954 | 0.144 | Stritzinger et al. (2011) |
| 2005am | NGC 2811 | SBa | 2368 | 0.778 | 0.056 | Contreras et al. (2010) |
| 2005bc | NGC 5698 | SBd | 3679 | 0.830 | 0.377 | Ganeshalingam et al. (2010) |
| 2005bo | NGC 4708 | SAab | 4166 | 0.852 | 0.243 | Ganeshalingam et al. (2010); Contreras et al. (2010) |
| 2005cf | MCG -01-39-03 | S0 ⁷ | 1937 | 0.995 | -0.015 | Wang et al. (2009) |
| 2005el | NGC 1819 | SB0 ⁸ | 4470 | 0.886 | -0.088 | Contreras et al. (2010) |
| 2005ke | NGC 1371 | SABa | 1463 | 0.677 | 0.653 | Hicken et al. (2009); Stritzinger et al. (2011) |
| 2006D | MCG -01-33-34 | SABab | 2556 | 0.818 | 0.105 | Stritzinger et al. (2011) |
| 2006N | MCG +11-08-12 | ? | 4280 | 0.795 | 0.027 | Hicken et al. (2009) |
| 2006X | NGC 4321 | SABbc | 1571 | 0.995 | 1.196 | Stritzinger et al. (2011) |
| 2006ax | NGC 3663 | SAbc | 5018 | 0.984 | -0.089 | Hicken et al. (2009); Stritzinger et al. (2011) |
| 2006ce | NGC 908 | SAc | 1509 | ... | ... | ... |
| 2006mq | ESO 494-G26 | SABb | 968 | ... | ... | ... |
| 2006ou | UGC 6588 | Sbc | 4047 | 1.393 | 0.345 | Hicken et al. (2012) |
| 2007N | MCG -01-33-12 | SAa | 3861 | 0.524 | 0.988 | Hicken et al. (2009); Stritzinger et al. (2011) |

during February 2010. WFI has a pixel scale of 0.238'' per pixel.

While the exact details of observing strategy changed slightly between different telescopes and instruments, overall procedures were very similar. Generally three 300 second H α exposures were obtained, followed by one 300 second broad-band R -band images. Standard imaging reduction techniques were employed using IRAF⁹ to first bias-subtract then flat-field all science frames. A range of foreground stars were then used to obtain a scaling factor

between the narrow and broad-band observations. After scaling, the broad-band images were subtracted from the H α observations. This leaves only the H α line emission within host galaxies, ready for analysis. Finally, images were astrometrically calibrated using the *Starlink* package ASTROM, enabling sub-arcsecond location of the SN explosion sites.

2.4 GALEX data

H α line emission within galaxies traces the most recent, on-going SF regions of ages less than 10 Myrs. Given that this is a much shorter timescale than even the youngest hypothesised SN Ia

⁹ IRAF is distributed by the National Optical Astronomy Observatory, which is operated by the Association of Universities for Research in Astronomy (AURA) under cooperative agreement with the National Science Foundation.

Table 1. *Continued...*

| SN | Host galaxy | Galaxy type | V_r (kms $^{-1}$) | Stretch | $(B-V)_{max}$ | References |
|--------|-------------|-------------|----------------------|---------|---------------|--|
| 2007S | UGC 5378 | Sb | 4161 | 1.095 | 0.116 | Hicken et al. (2009); Stritzinger et al. (2011) |
| 2007af | NGC 5584 | SABcd | 1638 | 0.953 | 0.073 | Hicken et al. (2009); Stritzinger et al. (2011) |
| 2007bm | NGC 3672 | SAC | 1862 | 0.922 | 0.474 | Hicken et al. (2009); Stritzinger et al. (2011) |
| 2008bi | NGC 2618 | SAab | 4031 | ... | ... | ... |
| 2008fv | NGC 3147 | SABc | 2802 | 1.104 | 0.165 | Tsvetkov & Elenin (2010); Biscardi et al. (2012) |
| 2009ag | ESO 492-G02 | SAb | 2590 | 0.978 | 0.124 | Unpublished, Carnegie Supernova Project |
| 2009ds | NGC 3905 | SBc | 5774 | 1.144 | 0.073 | Hicken et al. (2012) |
| 2009ig | NGC 1015 | SBa | 2629 | 1.075 | 0.140 | Foley et al. (2012b); Hicken et al. (2012) |
| 2010eb | NGC 488 | SAb | 2272 | ... | ... | ... |
| 2011B | NGC 2655 | SAB0/a | 1400 | ... | ... | ... |
| 2011ao | IC 2973 | SBd | 3210 | ... | ... | ... |
| 2011ek | NGC 918 | SABc | 1507 | ... | ... | ... |
| 2011dm | UGC 11861 | SABdm | 481 | ... | ... | ... |
| 2011dx | NGC 1376 | SACd | 4153 | ... | ... | ... |

Table 1. Information on the SN sample analysed in this work, together with estimated light-curve parameters and references for photometry. In the first column we list the SN name, followed by the host galaxy in column 2. Then in columns 3 and 4 respectively we list the Hubble type and recession velocity of each host galaxy (information taken from NED: <http://ned.ipac.caltech.edu/>). This is followed by the derived light-curve parameters for each SN: stretch followed by $(B-V)_{max}$ (the $B-V$ colour at maximum light). In column 7 we list the reference for SN photometric data (where we only include data if the light-curve fits passed our selection criteria).

¹Classification from IAU SN catalogue

²Classification as SN Ia from Sandage & Tammann (1993)

³While this galaxy is classed as Hubble type S0 (i.e. no, or very little SF), there is definitely large amounts of detected H α line emission produced by on-going SF

⁴Galaxy is classified as S0, but significant on-going SF is detected

⁵Galaxy is classified as S0, but significant on-going SF is detected

progenitors, we also choose to investigate the association of SN Ia explosion sites with SF of older ages. Near-UV emission within galaxies is thought to trace SF out to older ages (~ 100 Myr, see e.g. Gogarten et al. 2009). In the rest of the manuscript we will refer to near-UV imaging as tracing recent SF (in place of on-going with respect to that traced by H α). We searched the *GALEX* archive for near-UV images of our sample. Data were available for 74 SN Ia host galaxies and *GALEX* near-UV ‘intensity maps’ were obtained, which come astrometrically calibrated ready for analysis. These data have scales of $1''$ per pixel.

2.5 INT B -band data

B -band imaging was obtained with the WFC on the Isaac Newton Telescope (INT). Exposure times of ~ 500 seconds were employed and the WFC gives images of $0.333''$ per pixel scale. Standard imaging reduction techniques were employed to first bias-subtract then flat-field all science frames. Images were then astrometrically calibrated and accurate SN positions on reduced images were obtained.

2.6 NOT nearIR data

To obtain near-IR J - and K -band imaging the Nordic Optical Telescope (NOT) was employed using NOTCam. The instrument was used in wide field imaging mode which results in images with a FOV of $4' \times 4'$ and a pixel scale of $0.234''$ per pixel. A total J -band exposure time of 200 seconds was used, split into

4×50 second exposures. To account for the varying near-IR sky, frames offset from host galaxies were observed with the same exposure times as those used for science frames. Therefore 50 second exposures were taken on target, then offsets of $250''$ were applied to slew to sky positions. Within this sequence positions were dithered by $10''$ to remove stars from the sky frames and bad pixel defects on the detector. A similar process was employed for the K -band images with a total exposure time of 900 seconds split into 9×100 second exposures. Differential flat fields were obtained at either the start or the end of each observing night. Sky flats with low count levels were subtracted from similar frames with high levels and then the resulting flat field was normalised. Each subsequent sky frame was subtracted from its corresponding science frame. Each resulting sky-subtracted science frame was then divided by the normalised flat field. These resulting frames were then combined using median stacking. Images were then astrometrically calibrated as above. However, in many cases there were insufficient stars within the relatively small field of view of NOTCam to enable an astrometric solution. In these cases SN positions were calculated using offsets of SN coordinates from galaxy centres (with SN positions being taken from either the IAU SN list or NED, and galaxy centre coordinates taken from NED). Offsets were transformed to NOTCam pixel x and y offsets, and SN positions on the images were calculated using the peak of the J - or K -band flux on each image as the galaxy centre. To check the validity of this process, SN positions were also calculated in this way for images where an astrometric calibration was possible and the two methods were compared. In general SN pixel positions were consistent between the two methods, and NCR values (see below) were also consistent between the two pixel coordinate

values. The difference in the mean NCR values between the 21 SNe where the above comparison was possible in the J -band is 0.008, while for 20 SNe in the K -band the difference is 0.023.

2.7 Stellar populations traced by different wavebands

In this work we analyse the association of SNe Ia within star-forming hosts with galaxy light distribution in a range from $H\alpha$ through optical wave-bands to K -band near-IR observations. Each waveband analysed ($H\alpha$, near-UV, B -, R -, J - and K -band) traces different stellar population properties. $H\alpha$ emission traces SF on the shortest timescales of less than ~ 10 Myr. Near-UV emission traces SF on longer timescales out to ~ 100 Myr. When one moves to analyse broad-band observations at longer wavelengths direct age constraints become less clear. However, stellar population models appear to be in agreement that as one moves redwards then the older stellar mass of a stellar population/galaxy starts to contribute more significantly (see e.g. Worthey 1994, and Schawinski et al. 2007 who used the models of Maraston 2005). While it is generally assumed that young populations still dominate the flux detected through the B -band filter, the K -band light in most stellar populations is assumed to be dominated by the old stellar mass of that population (e.g. Mannucci et al. 2005).¹⁰ Following the above, we can speculate that if a SN distribution better traces that flux observed through a redder filter, then the dominant age of the progenitor population may be larger than that of a distribution which traces flux observed through a bluer filter. The above is obviously only a first order approximation, and one should be careful to draw strong conclusions following these arguments, especially given the effects of metallicity and extinction. However, in the following sections we will use this argument as a guide to understand the distributions derived, while stressing the uncertainties involved. In § 5.1.1 we present further constraints on the stellar population properties probed by our broad-band images.

3 ANALYSIS METHODS

The procedures for obtaining results from the statistical methods we use here, were first presented in James & Anderson (2006), and have been further outlined in their application to CC SN host galaxy samples in Anderson & James (2008), Anderson & James (2009); Habergham et al. (2010); Anderson et al. (2012); Habergham et al. (2012) and Habergham et al. (2014). Below we briefly outline our methods, but refer the reader to those previous publications for more detailed documentation.

3.1 Pixel statistics

In James & Anderson (2006), a pixel statistics method was introduced which was created to give a quantitative measure of the association of individual SNe to the underlying SF present within galaxies. This method produces, for each pixel within an

¹⁰ While Kangas et al. (2013) claimed that the K -band light in their galaxy sample may be tracing recent SF, this was due to their sample being of infrared-bright starburst galaxies, significantly distinct from the current sample.

image a value (dubbed ‘NCR’, Anderson & James 2008) between 0 and 1 which indicates where within the overall host galaxy SF distribution each pixel is found (note a very similar technique was independently developed by Fruchter et al. 2006). Images are first trimmed to remove non-galaxy regions of the field of view, and are then binned 3×3 (in order to reduce the affects of inaccurate SN coordinates and/or image alignment)¹¹. Pixels within each image are then ordered in terms of increasing count. From this ordered list we then form the cumulative distribution. Each pixel is then assigned an ‘NCR’ value by dividing the cumulative pixel count by the total of the cumulative distribution. All pixels forming part of the negative cumulative distribution are set to an NCR value of zero (either sky or zero flux pixels). Hence, all pixels have a value between 0 and 1, where a value of 0 indicates that the pixel is consistent with zero flux or sky values, whereas a pixel value of 1 means that the pixel has the highest flux count within the image. To build up NCR statistics for SN populations one simply takes the pixel where each SN falls and calculates its corresponding NCR value.

In the case of the current sample we apply this technique to each SN with respect to its $H\alpha$ image, and in addition with respect to its *GALEX* near-UV image, broad-band optical B and R images, and near-IR J - and K -band images. The resulting NCR values are listed in Table A1. Any population which directly follows the spatial distribution of light traced by each wave-band will show a flat distribution of NCR values with a mean value of 0.5. Whether a distribution follows such a one-to-one relation or not, then provides constraints on progenitor properties. In the cumulative plots below if a distribution accurately traces the light detected through a given filter, then one expects the distribution to follow the diagonal one-to-one line shown on each plot.

3.1.1 Spatial resolution

During the above description of our data sets, we have detailed the pixel scale of each distinct set of observations. During our processing of the host galaxy images, most data are binned 3×3 which means all images (UV through to near-IR) have NCR values which probe counts at a detector resolution of $\sim 1''$. However, in some cases the seeing during observations was considerably worse than this. Of all observations the image quality in the B -band was the worst, hence we use these data to present a limiting case of the spatial resolutions probed within galaxies through our NCR statistic. The median seeing as measured on B -band images was $1.6''$. The median recession velocity of our galaxy sample is 2647 kms^{-1} , which equates to a distance 36.3 Mpc . These two values give a median spatial resolution probed within galaxies of $\sim 280 \text{ pc}$. Hence, we resolve SN Ia host galaxies into a significant number of elements through our pixel statistics.

3.2 Radial analysis

While pixel statistics can give one information on the stellar population at exact explosion sites, SNe Ia have significant delay times and hence are likely to explode at considerable distances from their birth sites. One method to further explore the environments of SNe is to investigate where they explode with respect to the radial

¹¹ As the near-UV images have an initial pixel scale of $1''$ per pixel, these data were not binned.

distribution of different stellar populations. Within star-forming galaxies different age and metallicity stellar populations are found at different characteristic galactocentric radial positions. Therefore one can investigate where SNe are found within these more generalised galaxy trends, and further infer progenitor properties.

In James & Anderson (2006) we introduced a statistical radial analysis of SNe to those of stellar populations as traced by the continuum R -band light, and the $H\alpha$ emission respectively. To obtain these ‘ Fr ’ fractional flux values one proceeds in the following fashion. For each host galaxy elliptical apertures of increasing size are produced, centred on the galaxy central coordinates, and calculated using the position angle and ratio of major to minor axis of the galaxy (taken from NED). One then finds the aperture which just includes the SN position. The flux (both of the narrow and broad-band emission) within that aperture is then calculated, and normalised to the total galaxy emission by dividing by the flux within an aperture where the cumulative flux of the galaxy has become constant as one goes to larger galactocentric radii. Hence, each SN has a radial value corresponding to the continuum R -band light (Fr_R), and one corresponding to $H\alpha$ emission ($Fr_{H\alpha}$) between 0 and 1. A SN having a Fr value 0 would indicate that the SN exploded at the central peak $H\alpha$ or R -band pixel of the galaxy, while a value of 1 means that the SN falls on an outer region where the galaxy flux is negligible above the sky. Fr_R and $Fr_{H\alpha}$ SN Ia distributions are hence built. If a SN population directly follows the radial distribution of the broad- or narrow-band light, then the distribution of Fr values is expected to be flat. Therefore, we can investigate how the different samples are associated with the radial positions of different stellar populations. These techniques have been applied to CC SN samples in Anderson & James (2009); Habergham et al. (2010, 2012) and Habergham et al. (2014).

4 RESULTS

4.1 Pixel statistics

4.1.1 $H\alpha$

We present the overall SNe Ia $H\alpha$ NCR pixel distribution with respect to other main SN types in Figure 1 (note, an in-depth analysis of the CC SN sample was presented in Anderson et al. 2012). It is immediately apparent that SNe Ia show the lowest degree of association with the on-going SF (as seen previously by Bartunov et al. 1994, James & Anderson 2006 and most recently Galbany et al. 2014). This is to be expected if, as generally assumed, SNe Ia arise from some system containing a WD, i.e. a relatively old progenitor population. The mean $H\alpha$ NCR value (98 events¹²) is 0.157, with a standard deviation of 0.253, and a standard error on the mean of 0.026. This compares to mean values of 0.254 (162.5 SNe), 0.303 (40.5) and 0.469 (52), for the SN II, SN Ib and SN Ic distributions respectively. Nearly 60% of SNe Ia within star-forming galaxies fall on zero $H\alpha$ flux (down to the limits of our observations, see Anderson et al. 2012). Using a Kolmogorov-Smirnov test (KS-test) we find that there is less than a 0.1% probability that the SN Ia and SN II distributions are drawn from the same parent population. The SN Ia distribution does not follow the on-going SF within galaxies.

¹² Note that not all SNe in the sample have both NCR and Fr values, hence this value is lower than the 102 stated for the full sample of events earlier.

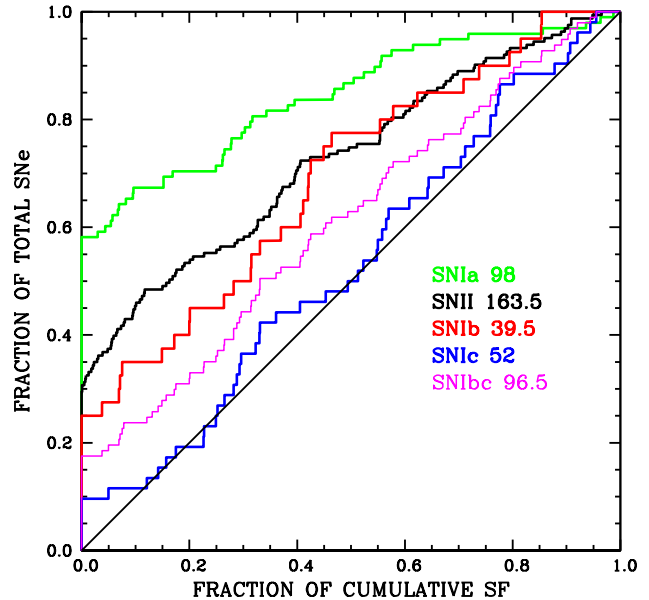


Figure 1. Cumulative $H\alpha$ pixel statistics distributions of the main SN types. As distributions move away to the upper left from the black diagonal (a hypothetical distribution, infinite in size, that accurately traces the underlying on-going SF), they are showing a lower association to the emission. (We note that this plot is the same as that presented in Anderson et al. 2012.)

Given that $H\alpha$ emission is generally thought to be produced from the ionising flux from stars less than 10 Myr old (Kennicutt 1998), this result is consistent with even the youngest predicted timescales for SN Ia progenitors (see e.g. Aubourg et al. 2008).

4.1.2 Near-UV

In Fig. 2 the cumulative NCR distributions are shown for 74 SNe Ia, with respect to both $H\alpha$, and *GALEX* near-UV emission. The SN Ia distribution shows a higher degree of association to the UV emission than that of $H\alpha$. However, it still appears that SNe Ia do not accurately trace recent SF. The mean near-UV NCR value is 0.292 with a standard deviation of 0.292 and a standard error on the mean of 0.034. This compares to a mean $H\alpha$ NCR value, for the same 74 events of 0.175 (standard deviation of 0.224, standard error on the mean of 0.026). Using a KS-test we find that there is a 0.5% chance that the SN Ia distribution shows the same degree of association to both the $H\alpha$ and near-UV emission. We also find that there is less than 0.5% chance that the SN Ia and SN IIP distributions, with respect to the near-UV emission, are drawn from the same parent population. Finally, the SN Ia near-UV distribution has a less than 0.1% chance of being drawn from a flat distribution, i.e. one that accurately traces the recent SF. This result suggests that at least the majority of SNe Ia found within star-forming galaxies do not explode on the timescales of <100 Myr traced by near-UV emission (Gogarten et al. 2009).

4.1.3 Multi wave-band NCR statistics

In Fig. 3 we present the NCR distributions of SNe Ia for multiple wavelength observations. The mean NCR values together with KS-test results of each distribution between that wave-band and a flat distribution are presented in Table 2. The SN Ia population

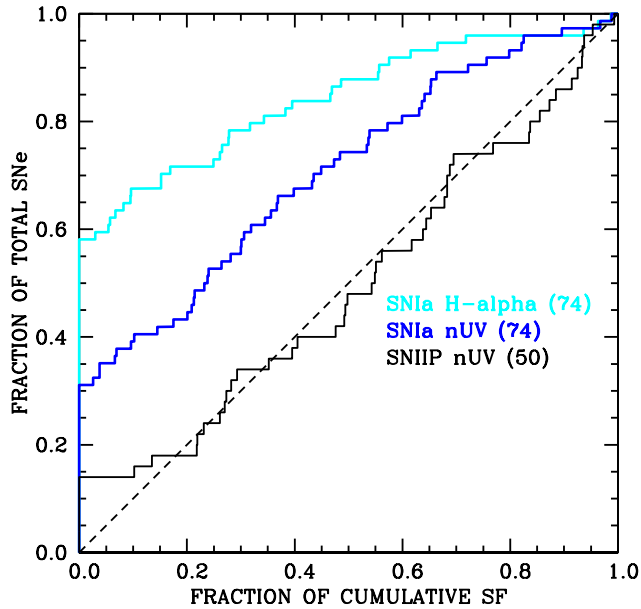


Figure 2. Cumulative distribution NCR plot showing the SN Ia population with respect to $H\alpha$ and near-UV emission of their host galaxies. For reference the SN IIP distribution with respect to near-UV emission is shown in solid black (taken from Anderson et al. 2012).

best traces the B -band host galaxy light, followed by the R -band light distribution. The SN Ia population does not follow the host galaxy light distribution in $H\alpha$, near-UV, nor the J - and K -bands. We speculate that this indicates that the SN Ia progenitor population in spiral galaxies does not arise from either the very young populations of less than a few 100 Myrs (that traced by $H\alpha$ and near-UV emission), but neither is it dominated by long lived population of several Gyrs (i.e. that traced by the J - and K -band light). The fact that the SN Ia population most closely follows the B -band light indicates that the progenitor population in late-type galaxies is dominated by relatively young systems.

It is also interesting to note how the different wave-band distributions compare to each other with respect to the values of individual SNe. Using the Pearson’s test for correlation, we find that nearly all wave-bands NCR values show significant correlation¹³. This means that if a SN has an NCR value near the top (or bottom) of the distribution in e.g. the R -band, then it is likely to have an NCR value near the top (or bottom) of the distribution in e.g. $H\alpha$, although the absolute NCR values may be significantly offset. The only wavebands that do not show significant correlation are: K and near-UV; K and $H\alpha$; and perhaps surprisingly near-UV and $H\alpha$. While a full discussion of the significance of these trends is beyond the scope of this paper, one may speculate that this indicates that while there are differences between the stellar populations traced by these different observations, the populations cluster together, i.e. where one finds significant flux of stellar light (e.g. B - and R -band) one also finds peaks of SF ($H\alpha$ and near-UV). An analysis comparing pixel statistics between different wave-bands, and including all host galaxy pixels (i.e. not just those where SNe have exploded),

¹³ Where we define significant correlation as a Pearson’s r -value higher than 0.5.

| Imaging band | Number of SNe | Mean NCR | KS-test from flat distribution |
|--------------|---------------|----------|--------------------------------|
| $H\alpha$ | 98 | 0.157 | <0.1% |
| near-UV | 74 | 0.292 | <0.1% |
| B | 43 | 0.498 | >10% |
| R | 80 | 0.415 | ~5% |
| J | 45 | 0.345 | ~0.5% |
| K | 45 | 0.293 | <0.1% |

Table 2. NCR statistics for the 6 distinct wave-band analyses. In the first column the wave-band is indicated, followed by the number of SNe and host galaxies analysed in column 2. In column 3 the mean NCR value for each distribution is presented. Finally in column 4 the chance possibility of each distribution following a flat distribution is listed, as calculated using the KS-test. (Note, if we only analyse those SNe common to all wave-bands, the results are completely consistent with the above.)

may give interesting constraints galaxy SFHs. Such analysis, independent of SN studies, will be the focus of future work.

4.1.4 $H\alpha$ pixel statistics with respect to event properties

SNe Ia light-curve stretch values were estimated for 56 SNe within the sample, as outlined in § 2.1. We split this sample by the median stretch of 0.978 and resulting $H\alpha$ NCR cumulative distributions are shown in Fig. 4. No statistical difference between the two distributions is found. We were able to estimate $(B-V)_{max}$ values for 54 SNe and the sample is split by the median $(B-V)_{max}$ value of 0.111. The results from this analysis are presented in Fig. 5. ‘Redder’ events (those with $(B-V)_{max} > 0.111$) show a higher degree of association with $H\alpha$ than ‘bluer’ SNe (similar to the results found by Rigault et al. 2013). The mean $H\alpha$ NCR for the ‘red’ events is 0.209 (0.266, 0.052), while for the ‘blue’ events the mean is 0.070 (0.140, 0.027). Using a KS-test, this difference is significant at the ~10% level (in addition the mean values are different at the 3 sigma level). An underlying difference in the sense that ‘redder’ SNe Ia are more likely to be found nearer/within bright H II regions could be explained by the fact that within bright H II regions SNe are likely to suffer from higher degrees of line of sight extinction. It is also possible that progenitor properties could play some role.

4.1.5 Near UV pixel statistics with respect to event properties

Now we repeat the analysis presented in the previous section but with respect to near-UV in place of $H\alpha$ emission. There are some host galaxies within our $H\alpha$ sample that do not have corresponding near-UV images available. Therefore for this sub-sample with available images we re-calculate median stretch and $(B-V)_{max}$ values, finding 0.984 and 0.105 respectively. The mean near-UV NCR values for the stretch distributions are 0.253 (0.267, 0.057) and 0.266 (0.307, 0.067), for the high and low stretch SNe respectively, i.e. we find no statistical difference between the association of low and high stretch to recent SF, as shown in Fig. 6. This suggests that even the most ‘prompt’ SNe Ia found within star-forming galaxies –which are likely to be related to the higher stretch population– do not have delay times less than a few 100 Myrs. The $(B-V)_{max}$ distributions, when split by the median value of 0.105 are shown in Fig. 7. It appears that ‘redder’ events show a higher degree of association to the near-UV emission than the ‘bluer’ ones. Again

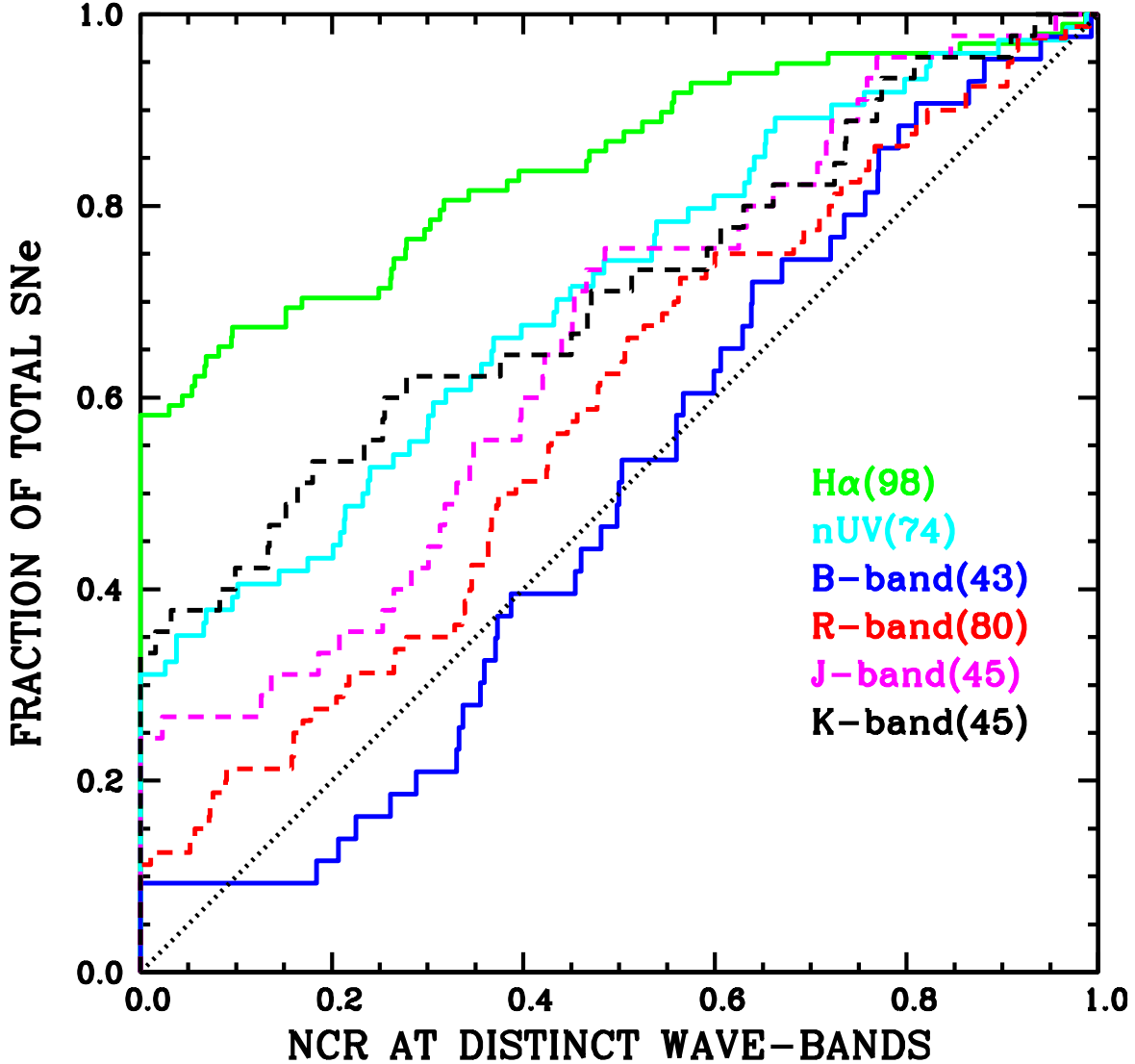


Figure 3. NCR distributions for SNe Ia with respect to 6 different wave-band host galaxy images (in star-forming galaxies).

this trend is probably most easily explained by these SNe suffering from higher extinction from line of sight material, but we stress the possibility of progenitor properties playing some role. Below we further investigate the environments of the ‘reddest’ events in our sample. We note that if we repeat the above analysis with respect to the other wavebands analysed above we do not observe any significant differences between the stretch or colour samples.

4.2 Radial analysis

Here we present results from the fractional radial analysis, the methods for which were outlined in § 3. We ask two main questions: 1) does the radial distribution of SNe Ia within host galaxies accurately trace the *R*-band stellar continuum population, or more accurately the $H\alpha$ emission, a tracer of the on-going SF within host galaxies? 2) If we split the SN Ia distribution by light-curve param-

eters, do specific types of SNe Ia occur at different characteristic radial positions within galaxies? We start by analysing the overall radial distributions¹⁴.

4.2.1 Overall SN Ia radial distributions

In Fig. 8 a histogram of the radial distribution of SN Ia with respect to the stellar continuum of their hosts is presented. The mean

¹⁴ We do not present *Fr* distributions with respect to the other wave-bands analysed through our NCR method above. While pixels statistics give specific information at the exact location of each SNe, the *Fr* analysis is a much more crude environment property estimator, where differences between similar wave-length observations are not significant. In order to not overload the reader with additional analysis and figures we choose present only the $H\alpha$ and *R*-band analysis in this section.

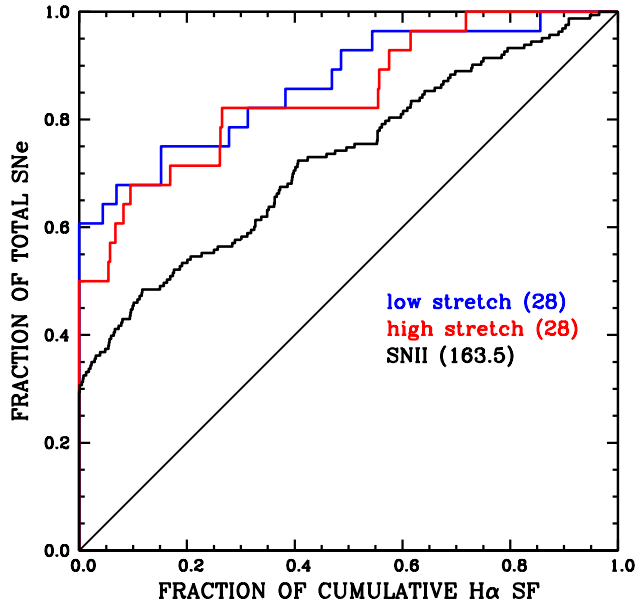


Figure 4. $H\alpha$ cumulative pixel statistics plot with SNe Ia (in star-forming galaxies) split into those above and below the median stretch value of 0.978. The SN II distribution is shown for reference

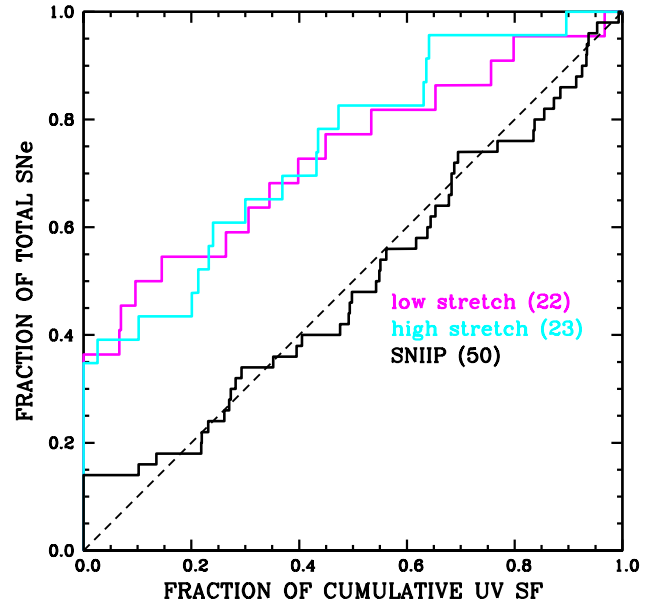


Figure 6. *GALEX* near-UV cumulative pixel statistics plot with SNe Ia (in star-forming galaxies) split into those above and below the median stretch value of the sample of 0.984. The SN IIP distribution (with respect to near-UV emission) is shown for reference

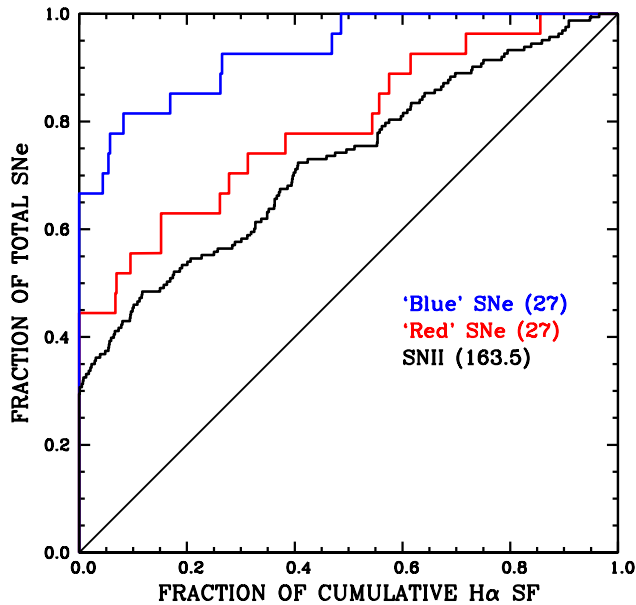


Figure 5. $H\alpha$ cumulative pixel statistics plot with SNe Ia (in star-forming galaxies) split into those above and below the median $(B-V)_{max}$ of 0.111. For reference the SN II distribution is also shown.

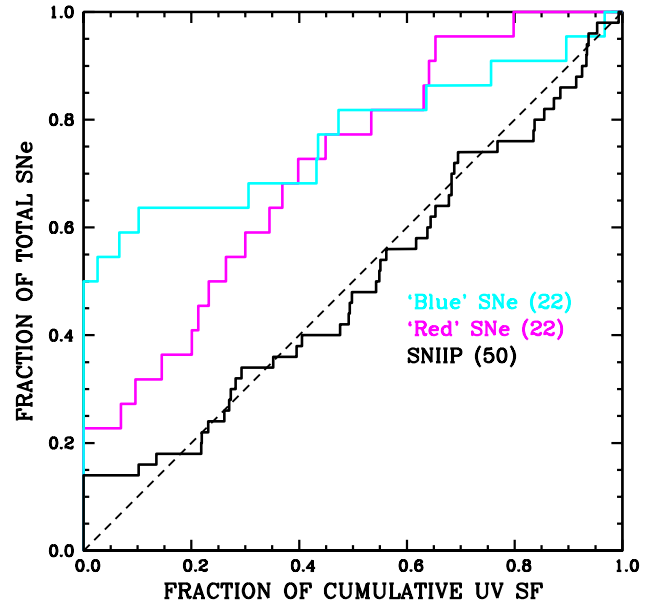


Figure 7. *GALEX* near-UV cumulative pixel statistics plot with SNe Ia (in star-forming galaxies) split into those above and below the median $(B-V)_{max}$ of 0.105. The SN IIP distribution is shown for reference

F_{Rr} for the overall SN Ia distribution (99 SNe) is 0.554 (standard deviation of 0.261, standard error on the mean of 0.026). Hence, the distribution appears to be slightly biased towards larger radial distances when compared to the R -band light. There appears to be a central deficit of SNe Ia, and indeed this deficit is seen when we apply a KS-test between the SN Ia F_{Rr} and a flat distribution. We find a $\sim 7\%$ chance that the SNe Ia accurately traces the radial R -band distribution of their hosts. The easiest way to interpret this

result would be that it is solely a selection effect where SNe Ia go undetected in the central parts of galaxies due to higher levels of extinction and higher surface brightness. However, in Fig. 9 we show the SN Ia F_{Rr} plot in a cumulative distribution, compared to that of 185 SNe II and 97 SNe Ibc (these results have been presented in Anderson & James 2009; Habbergham et al. 2010, 2012). This shows that while the SNe II also have a central deficit,

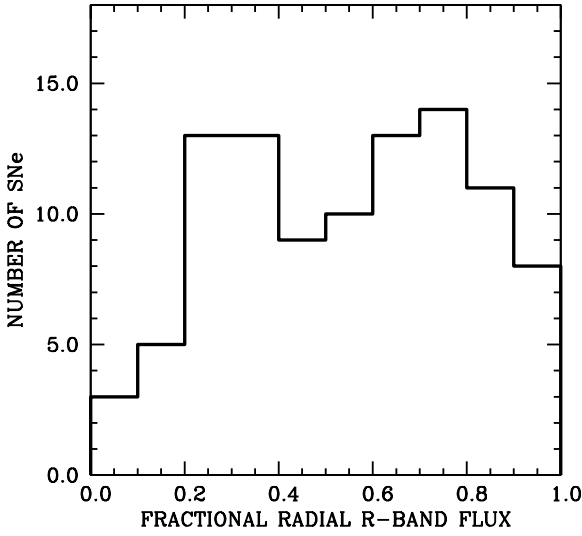


Figure 8. Histogram of fractional radial distribution of the overall SN Ia population (99 SNe in star-forming galaxies) with respect to the R -band light distribution of their hosts.

SNe Ibc do not show any such deficit. Given that SNe Ia are generally more luminous than SNe Ibc (meaning that any selection effect against finding SNe in the central parts of galaxies should be worse for the latter), this suggests that the lack of SNe Ia found within the central parts of galaxies is a real, intrinsic observation.

In Fig. 10 we show a histogram of the radial distribution of SNe Ia compared to the distribution of on-going SF of their hosts. The mean $Fr_{H\alpha}$ is 0.560 (0.313, 0.031). As for the distribution with respect to the R -band light, the SNe Ia appear to explode at slightly larger galactocentric distances with respect to $H\alpha$ emission. However, there is no large deficit in the central parts of the emission. This is also seen using a KS-test where the SN Ia distribution is consistent with being drawn from a flat distribution, i.e. one that accurately traces the radial distribution of $H\alpha$ emission. In Fig. 11 the SN Ia radial $H\alpha$ cumulative distribution is presented, compared to that of 185 SNe II and 97 SNe Ibc. SNe Ia appear to become more numerous per unit SF out to larger galactocentric radii than the CC SNe within our previously published samples.

4.2.2 Radial distributions of SNe Ia when split by light curve parameters

As was done for the pixel statistics analysis above, we now analyse whether there are differences in the radial distributions of SNe Ia when the sample is split by light-curve parameters. The sample is split by a median stretch of 0.984, and by the median $(B-V)_{max}$ of 0.106. In Figs. 12 and 13 histograms of the radial distributions of SNe Ia with respect to the R -band and $H\alpha$ light are shown, with the sample split by stretch. In Figs. 14 and 15 histograms of the radial distributions are presented with the sample split by $(B-V)_{max}$. The mean values (together with standard deviations and standard errors on the mean), plus KS-test percentage values, and sigma differences between means are listed in Table 3.

The most significant difference between these various popula-

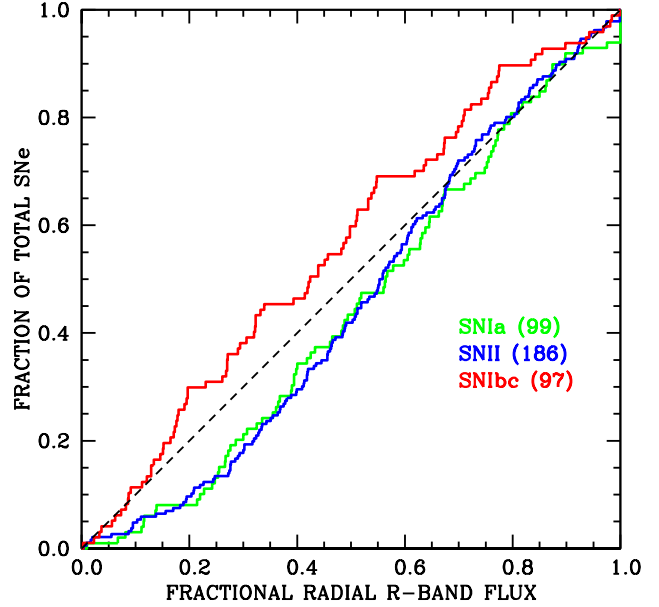


Figure 9. Cumulative distribution of the Fr_R values of SNe Ia (in star-forming galaxies) and the CC SN types, SN II and SN Ibc, with respect to the R -band light distribution within their host galaxies.

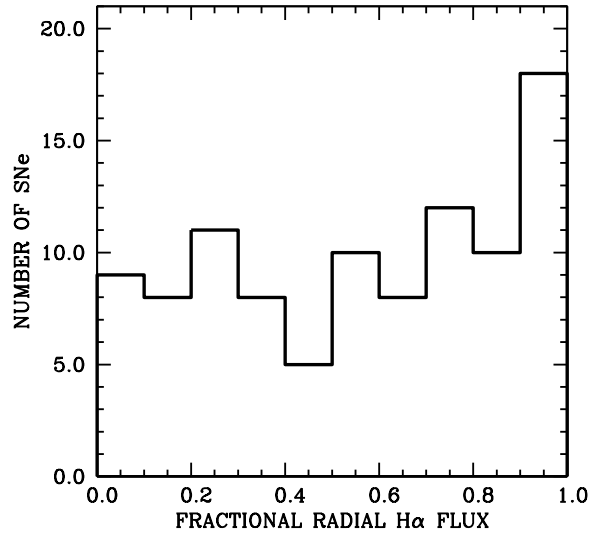


Figure 10. Histogram of fractional radial distribution of the overall SN Ia population (99 SNe in star-forming galaxies) with respect to the $H\alpha$ line emission distribution of their host galaxies.

tions is between the Fr_R distributions when split by SN colour. A KS-test shows the distributions to be different with a 0.3% chance probability of being drawn from the same underlying population. This difference is in the sense that ‘redder’ events are found more centrally within host galaxies, as also observed by Galbany et al. (2012).

| Distribution | N. of SNe | Mean Fr (stdev, sterr) | KS-test | sigma difference |
|-----------------------------------|-----------|--------------------------|---------|------------------|
| Fr_R high stretch | 27 | 0.562 (0.241, 0.047) | >10% | 0.08 |
| Fr_R low stretch | 28 | 0.557 (0.248, 0.048) | | |
| $Fr_{H\alpha}$ high stretch | 27 | 0.498 (0.302, 0.059) | >10% | 0.97 |
| $Fr_{H\alpha}$ low stretch | 28 | 0.581 (0.323, 0.061) | | |
| Fr_R red $(B-V)_{max}$ | 26 | 0.500 (0.245, 0.041) | 0.3% | 1.90 |
| Fr_R blue $(B-V)_{max}$ | 26 | 0.619 (0.234, 0.047) | | |
| $Fr_{H\alpha}$ red $(B-V)_{max}$ | 26 | 0.460 (0.311, 0.063) | >10% | 1.90 |
| $Fr_{H\alpha}$ blue $(B-V)_{max}$ | 26 | 0.625 (0.308, 0.062) | | |

Table 3. Mean Fr values for each of the 8 distributions, with respect to both the R -band and $H\alpha$ light. In column 1 the distribution name is given, followed by the number of events within that distribution in column 2. Then the mean Fr values are given together with their associated standard deviations and standard errors on the mean. Finally for each set of distributions (i.e. split by either light-curve stretch or colour) we list the KS-test probabilities that the two distributions are drawn from the same parent population, followed by the statistical difference (in terms of sigma) between the mean values of each population.

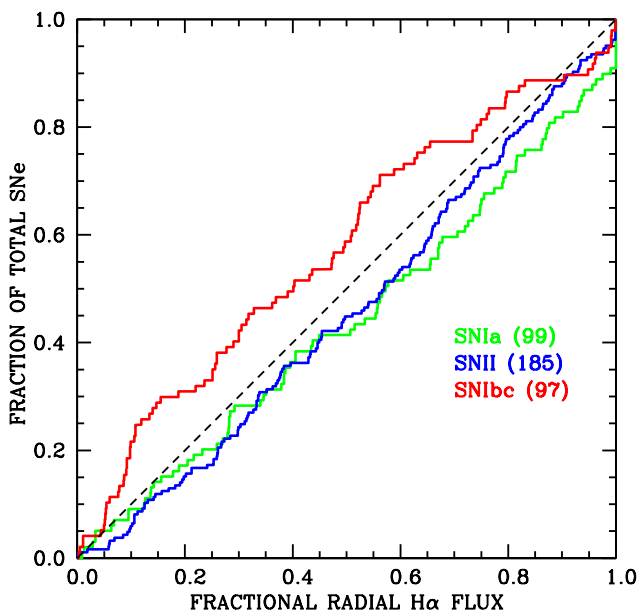


Figure 11. Cumulative distribution of the radial distribution of SNe Ia (in star-forming galaxies) and the CC SN types, SN II and SN Ibc, with respect to the $H\alpha$ emission distribution within their host galaxies.

4.3 The environments of the ‘reddest’ SNe Ia

It has been shown that ‘redder’ SNe are generally found to both fall on regions of more intense SF and in more central parts of galaxies than their ‘blue’ counterparts. If these results are due to line of sight ISM then one may ask if there are SNe which are significantly ‘red’ but *do not* fall on star-forming regions or in the central parts of their galaxies? We define ‘red’ SNe as those with a $(B-V)_{max}$ value higher than 0.5. We then compile the data for these SNe in Table 4 where we present SN colours together with their $H\alpha$ and near-UV NCR values, and their Fr_R and $Fr_{H\alpha}$ values. We find that these ‘reddest’ SNe indeed generally occur within bright H II regions (as indicated by their NCR values) and in more central regions. The mean $H\alpha$ NCR value for these 10 SNe is 0.232, higher than the 0.157 for the full sample. In addition, almost 60% of the full sample fall on regions of zero $H\alpha$ flux, while this falls to 40% for these 10 SNe. In terms of their radial positions, the mean Fr_R for this sub-

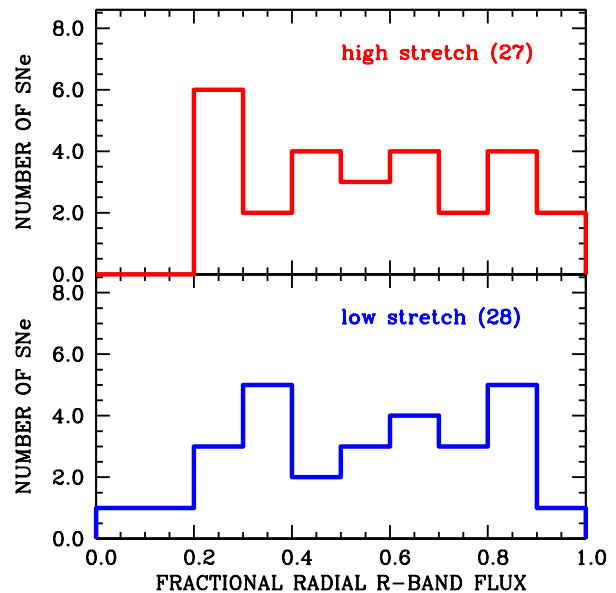


Figure 12. Histogram of fractional radial distribution of the SN Ia population (in star-forming galaxies) with respect to the R -band light distribution of their host galaxies, when split by the median stretch value of 0.984.

set of events is 0.408, compared to 0.554 for the full sample, and the difference is more extreme for $Fr_{H\alpha}$: 0.292 for the sub-sample, and 0.560 for the full sample. Looking closely at Table 4 there is only one SN where one may argue that the environmental properties cannot explain its ‘red’ colour: SN 2005ke (the rest of the sample either fall on regions of significant SF or in central regions).¹⁵ We note that this is the ‘bluest’ SN within this sub-sample. Below we further discuss the implications of this result.

5 DISCUSSION

In previous sections statistical distributions of SN Ia environments have been presented together with results characterising the prop-

¹⁵ Indeed, other than this SN *all* of the events within this sub-sample exploded within the central 50% of their host galaxy light.

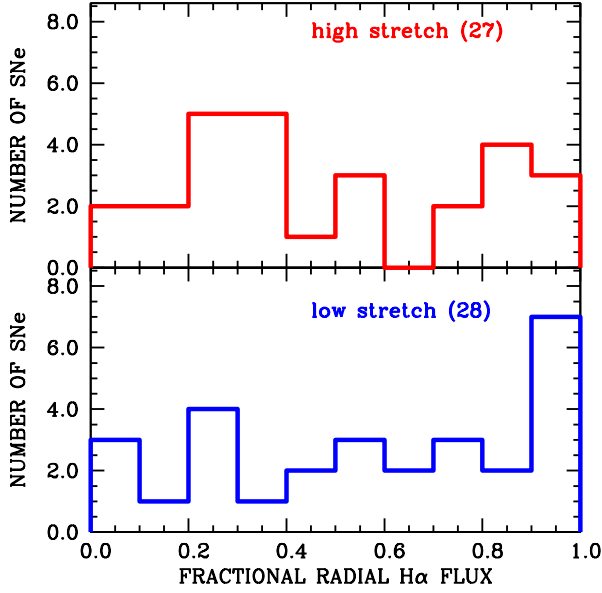


Figure 13. Histogram of fractional radial distribution of the SN Ia population (in star-forming galaxies) with respect to the $H\alpha$ emission distribution of their host galaxies, when split by the median stretch value of 0.984.

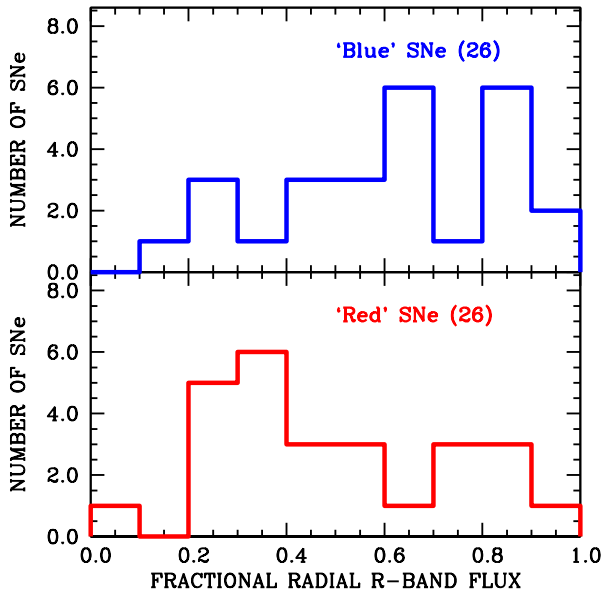


Figure 14. Histogram of fractional radial distribution of the SN Ia population (in star-forming galaxies) with respect to the R -band light distribution of their host galaxies, when split by the median $(B-V)_{max}$ of 0.106.

erties of the stellar light found in the vicinity of SNe Ia within star-forming galaxies. Now we further discuss how these results can be understood in terms of progenitor properties and SNe Ia diversity.

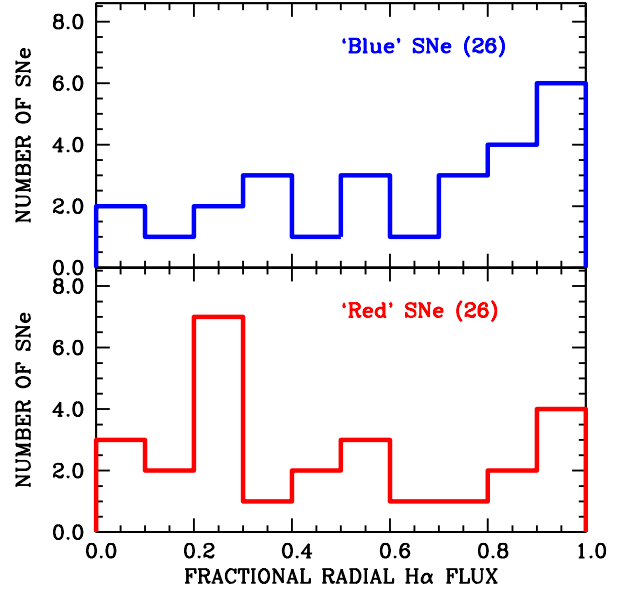


Figure 15. Histogram of fractional radial distribution of the SN Ia population (in star-forming galaxies) with respect to the $H\alpha$ emission distribution of their host galaxies, when split by the median $(B-V)_{max}$ of 0.106.

| SN | $(B-V)_{max}$ | NCR $H\alpha$ | NCR UV | Fr_R | $Fr_{H\alpha}$ |
|--------|---------------|---------------|--------|--------|----------------|
| 1986G | 0.839 | 0.069 | ... | ... | ... |
| 1995E | 0.679 | 0.000 | 0.345 | 0.394 | 0.284 |
| 1996ai | 1.553 | 0.615 | 0.232 | 0.325 | 0.292 |
| 1999bh | 0.872 | 0.856 | ... | 0.418 | 0.232 |
| 1999cl | 1.059 | 0.152 | 0.264 | ... | ... |
| 2003cg | 1.110 | 0.557 | 0.369 | 0.242 | 0.142 |
| 2005A | 0.986 | 0.000 | 0.398 | 0.255 | 0.136 |
| 2005ke | 0.653 | 0.000 | 0.069 | 0.861 | 0.815 |
| 2006X | 1.196 | 0.067 | 0.201 | ... | ... |
| 2007N | 0.988 | 0.000 | 0.000 | 0.361 | 0.282 |

Table 4. The environment statistics for the ‘reddest’ SNe Ia in the sample. Here we show all SNe which have $(B-V)_{max}$ higher than 0.5. In the first column the SN name is listed, followed by the $(B-V)_{max}$ in column 2. In columns 3 and 4 we present the NCR values derived from $H\alpha$ and near-UV imaging respectively. Then the Fr_R and $Fr_{H\alpha}$ values are listed in columns 5 and 6 respectively.

5.1 Implications for SN Ia progenitors

It has long been accepted that SNe Ia found within star-forming galaxies have shorter lifetimes than those found within elliptical galaxies, due to the longer lived population of the latter. Indeed, there is now significant evidence in the literature that late-type galaxies host brighter SNe Ia (Hamuy et al. 2000; Sullivan et al. 2006; Kelly et al. 2010; Sullivan et al. 2010; Lampeitl et al. 2010; Gupta et al. 2011; D’Andrea et al. 2011; Johansson et al. 2013; Hayden et al. 2013; Childress et al. 2013; Pan et al. 2014), and these events are generally assumed to form any ‘prompt’ progenitor channel. In the current work we have only included star-forming host galaxies within our sample. This is by design, as our main initial goal was to investigate the association of SNe of all types with host galaxy SF. Hence, we remove a large fraction the SN popu-

lation which is distinct from that found in our sample. However, late-type galaxies have much more diverse stellar populations than those found in ellipticals, and hence one may hope that environmental differences exist that can be used to constrain progenitor properties. These involve the ages traced by different wave-bands analysed, together with metallicity gradients within spiral galaxies, and in addition the wide range of line of sight extinction found within different regions of star-forming galaxies.

5.1.1 Constraints on SNe Ia progenitor ages

SN Ia do not trace the $H\alpha$ nor the near-UV emission, i.e. the on-going or recent SF. However, they do seem to trace the B -band light extremely well (see Fig. 3). Going further redwards they do not trace the J - or K -band light. Qualitatively, this suggests that the dominant progenitor population in late-type galaxies is neither extremely prompt, nor significantly delayed. We speculate that the population is dominated by progenitors with ages of several 100s of Myrs. As our technique is statistical in nature, we cannot rule out extreme young or extreme old progenitors for any given SN. However, our results suggest that the B -band light distribution within star-forming galaxies is consistent with the stellar population which traces the peak of the SN Ia delay time distribution (DTD). Indeed, it has been argued by Childress et al. (2014) that this where the great majority of SNe Ia will arise from within these galaxies. $H\alpha$ and near-UV emission trace stellar populations with ages of less than around 10 and 100 Myrs respectively. The fact that the SN Ia population investigated here does not follow the light of either tracer of SF constrains the majority of these progenitors to have delay-times significantly longer than these limits. The observation that SNe Ia in star-forming galaxies also does not trace the near-IR light distribution –as traced by J - and K -band observations– would also appear to constrain the majority of their progenitors to have significantly shorter delay-times than traced by these near-IR observations. While the SN population shows some degree of correlation with the R -band light, it best follows the B -band light. We use the output from the population synthesis models of Pietrinferni et al. (2004) to extract the population age where the peak flux coincides with the central wavelength of B -band filter observations (note, other such models give very similar results). We find that a population age of ~ 750 Myrs matches well the wavelength range probed by B -band observations (which is demonstrated with a different set of models in figure 9 of Bruzual & Charlot 2003). Hence, this constrains the peak age of progenitors within our star-forming galaxy sample to fall within a similar range.

Raskin et al. (2009), using similar pixel techniques to those used here (but confined to regions in the immediate vicinity of the SN), compared SN Ia environments to analytical galaxy models, concluding that even the ‘prompt’ SNe Ia progenitor channel exhibits a delay time of 200–500 Myrs, consistent with our more qualitative arguments above. An important point here is that Raskin et al. (2009) also commented that SNe Ia and CC SNe show a similar degree of association to the g -band light of their host galaxies. However, while we make no comparison between the two SN types with respect to g -band light (or more appropriately, B -band as analysed here), in Fig. 2 it is clear that SNe Ia do not follow the near-UV emission while SNe II (and other CC types to a higher degree, see Haberman et al. 2014) show almost a perfect one-to-one relation to the recent SF. Hence, this shows that indeed one can separate the two SN types using multi-wavelength pixel statistics analysed for complete galaxies.

While the above argues against a progenitor population dom-

inated by extremely young channels for the overall sample analysed, one may speculate that the ‘prompt’ channel is only a fraction of our sample. In § 4.1 we indeed separated the sample by ‘stretch’, where one would assume that the SNe with larger values (i.e. brighter events) are most likely to form the ‘prompt’ channel¹⁶. However, there is no difference in the association of the two SN groups with either on-going or recent SF. Hence, even the majority of the most ‘prompt’ SNe Ia in star-forming galaxies would appear to be constrained to have progenitors with delay times longer than at least 100 Myrs. We note, the statistical nature of our analysis does not rule out any particular SN having shorter lifetimes. However, we suggest that the relative rate of any population (if it indeed exists) must be quite small.

5.1.2 Radial distributions of SNe Ia: progenitor age or metallicity constraints?

In § 4.2 it was shown that the central parts of galaxies are underpopulated by SNe Ia, and that it appears unlikely that this is a selection effect given that SNe Ibc –which are intrinsically dimmer than SNe Ia– do not show any such deficit. This central deficit of SNe Ia with respect to CC SNe was also previously shown by Wang et al. (1997). In addition, as one goes out to larger galactocentric normalised distances there is a suggestion that per unit SF more SNe Ia are being produced (see Fig. 10). One can attempt to explain these results through both progenitor age and metallicity effects. In this section we explore both these possibilities.

A progenitor metallicity effect may manifest itself, when one considers that metallicity gradients are found within galaxies (central regions having higher abundances than outer regions, see e.g. Henry & Worthey 1999). Thus the above results could be interpreted in that SNe Ia prefer to explode within lower abundance regions of galaxies. Indeed there is some suggestion of such a trend in recent observational and theoretical works. Prieto et al. (2008) concluded that there is no significant low-metallicity threshold (below which SNe Ia are not produced) by investigating global host metallicities. Li et al. (2011) showed that the SN Ia rate per unit mass has a strong relation to host galaxy mass, with more events being produced per unit mass in lower mass galaxies. Quimby et al. (2012) also found an excess of dwarf hosts (i.e. low metallicity) in a sample produced by the non-targeted search of ROTSE-IIIb. These observational results were then used by Kistler et al. (2013), who argued that lower metallicity progenitors will lead to higher WD masses which then elevates the SN Ia rate in low metallicity environments as a higher fraction of WDs are able to explode as a SN Ia. Indeed, a prediction of Kistler et al. (2013) was that the SN Ia rate should be higher in the outer regions of galaxies, which is suggested by our work. It is important to note at this point the earlier theoretical work which in fact predicted the opposite to the above. Kobayashi et al. (1998) proposed that SD progenitors should show a preference for high metallicity because of a lower metallicity limit for the production of SNe Ia. This is related to the strong wind blown by the accreting WD, which was required for the progenitor to reach the Chandrasekhar mass. If metallicity is too low then the wind is too weak for the progenitor to evolve to explosion (Kobayashi et al. 1998). Observations (including our own) appear to rule out such a distinct metallicity effect. However,

¹⁶ We note that given our sample lacks any elliptical galaxy hosts, it is essentially dominated by moderate–stretch ‘prompt’ SNe in the traditional classification.

additional work is needed to further investigate this issue. One possibility is to measure the metallicity at the exact explosion site of SNe Ia. If SNe Ia indeed prefer higher/lower metallicity then one would expect that their explosion sites would have higher/lower values than average regions throughout their galaxies. Such analyses are now possible with the advent of wide field of view integral field spectrographs. It has also been shown that ‘redder’ events are found more centrally within galaxies. While we discuss this below in terms of progenitor age, and then line of sight extinction effects, it is also possible that this could be explained through a metallicity effect, which would imply that ‘redder’ SNe arise from higher metallicity progenitors.

Progenitor age could also be the explanation for our radial distribution results. Within star-forming spiral galaxies, in addition to metallicity gradients, one observes significant gradients in population SFHs. This is in the sense that the outer regions have SFHs dominated by younger populations, while more central regions have a much higher fraction of old stars. It has been observed that the SN Ia rate per unit mass is highly dependent on the colour of parent populations (galaxies), with Mannucci et al. (2005) showing that the rate per unit mass is much higher in galaxies with bluer colours. Hence, redder, older, more central stellar populations within galaxies have lower SN Ia rate per unit mass, providing an explanation for the lack of SNe in the central parts of the R -band light distribution of hosts. Indeed, this argument can also be used to explain that the elevated rate of SN Ia in low mass galaxies is due to a population age effect (rather than metallicity), as these galaxies are more actively star-forming, and hence SN Ia progenitor ages peak at the peak of the DTD, as outlined in Childress et al. (2014). If this second effect of progenitor age is the dominant factor which explains SN Ia environment properties, then one may argue that metallicity plays only a minor role. Indeed, there are now several investigations which argue that progenitor population age is the dominant parameter which correlates with Hubble residuals, and that there is insufficient evidence for any metallicity bias within SN Ia studies.

5.2 A SN Ia sample in exclusively star-forming galaxies

The currently analysed sample is formed exclusively by star-forming galaxies and lacks elliptical hosts. While the SN Ia rate per unit mass is significantly higher in star-forming galaxies (see e.g. Sullivan et al. 2006), ellipticals still produce a significant number of SNe Ia. Distinct SN Ia populations are found in ellipticals and in star-forming galaxies. The population within ellipticals is generally less luminous with lower stretch values. We have found that SN Ia stretch does not appear to correlate with environment *within* host galaxies. Given the classic result of a correlation between SN light-curve morphology with host galaxy type—that higher stretch SNe are found in later morphological types—one may therefore ask how we reconcile this with our result showing no environmental differences stretch separated samples. It could be that our sample is biased in such a way to remove those SNe driving the global stretch trend. To investigate we analyse host galaxy T-types¹⁷ for all SNe with estimated stretch values. In Fig. 16 we show the cumulative distributions of the SN Ia sample with respect to host galaxy type, separated by median stretch. The classic result still holds, in that the high stretch sub-sample has in general host galaxies of higher T-type. The difference between the two samples is significant at

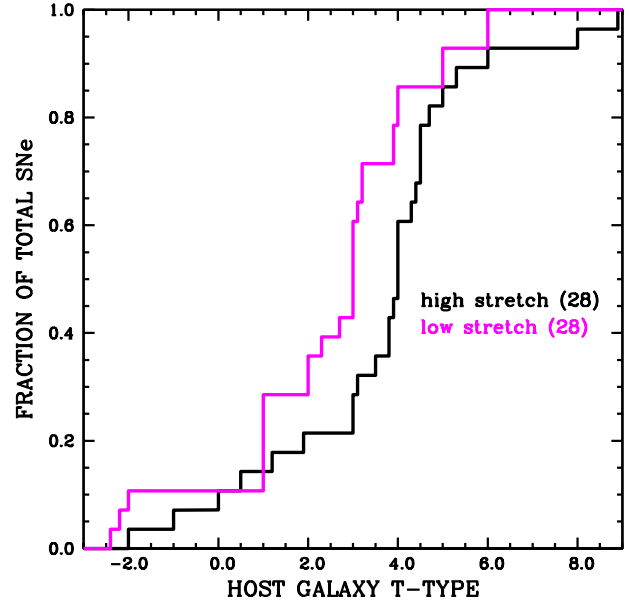


Figure 16. Cumulative plot showing the host galaxy T-type distribution of SNe Ia when divided into high and low stretch samples.

the 2.5% level when a KS-test is applied. We also investigate host T-type distributions when the sample is split by the median SN $(B-V)_{max}$ colour, and they are presented in Fig. 17. This shows the possibly surprising result that ‘redder’ SNe are found in earlier T-type hosts (significant at the $\sim 5\%$ level). If one assigns the majority of SN Ia colour diversity to ISM effects, then one would expect the opposite result. We note that a similar result was presented by Smith et al. (2012). This is possibly hinting at a metallicity effect, with ‘redder’ events occurring in higher metallicity (earlier Hubble type) galaxies.

In conclusion, while overall global host galaxy properties (such as age and metallicity) appear to affect the light-curve shape of SNe Ia, the specific stellar populations nearer to the explosion sites of these events do not seem to affect their properties. This is in contrast to CC SNe, where differences between global properties of host galaxies (see e.g. Hakobyan et al. 2014) are in general much smaller than differences of their nearby environments. The main driver of these differing results would appear to be the ages of the respective progenitors. CC SNe have lifetimes of at most several tens of Myrs and hence they have little time to move away from their parent stellar populations. On the other hand, SNe Ia most likely have progenitor delay times of at least several 100 Myrs, which gives both their progenitors time to move away from their birth sites, but also gives time for the population of stars at their birth sites to evolve significantly. This effectively washes out the information that can be gained on SN Ia progenitors from analysing the stellar populations at the exact explosion sites of SNe Ia.

5.3 SN colour with respect to environmental effects

One of our key findings is that ‘redder’ SNe are found to occur both nearer to bright H II regions, while at the same time closer to the centres of hosts than their ‘bluer’ counterparts. Given the results shown in § 4.3, one may worry that it is the reddest events which are driving these trends, where it is generally accepted that

¹⁷ Taken from the HyperLeda database: leda.univ-lyon1.fr.

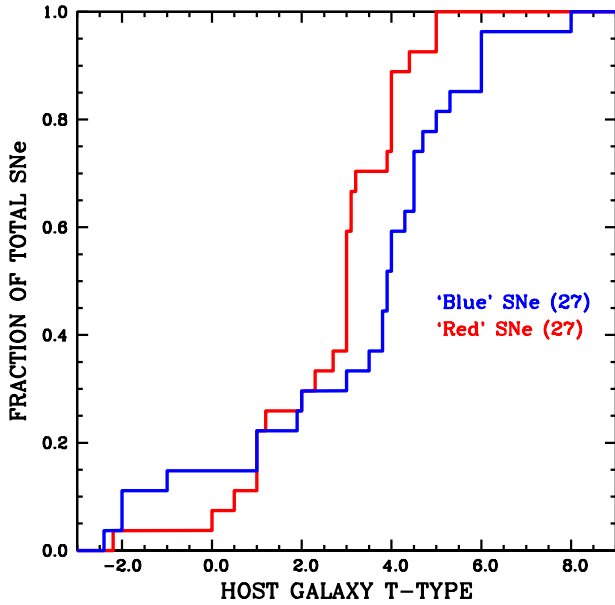


Figure 17. Cumulative plot showing the host galaxy T-type distributions of SNe Ia when divided into ‘red’ and ‘blue’ colour samples.

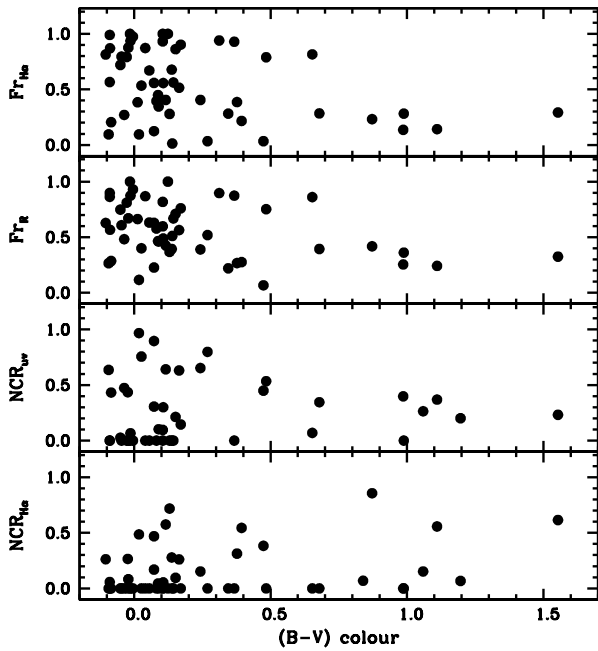


Figure 18. Environmental property indicators against $(B-V)_{max}$.

their ‘red’ colours do indeed arise from ISM extinction. To elucidate this issue we thus cut our sample to only include those SNe with $(B-V)_{max} < 0.2$, which leaves one with a more general sample similar to those usually used for cosmology. Again the sample is split by the median $(B-V)_{max}$. The above findings are completely robust to this further analysis. In this sub-set of events the ‘redder’ SNe are generally found to occur close to regions of $H\alpha$ SF, and at the same time within more central regions.

In Fig. 18 we present SN $(B-V)_{max}$ colours plotted against our

four main environment indicators: $NCR_{H\alpha}$, NCR_{nUV} , Fr_R , $Fr_{H\alpha}$. The vast majority of SNe Ia which have $H\alpha$ NCR values of zero are relatively ‘blue’ events. There is also a lack of ‘blue’ SNe with NCR values higher than 0.4: all SNe with negative $(B-V)_{max}$ values have NCR statistics lower than this value, however for ‘redder’ events there are many SNe with higher values. With respect to the UV NCR distribution, any trend with SN colour is much less clear, as already shown above. The one obvious observation is that again the majority of events with NCR values of zero are clustered around $(B-V)_{max}$ colours of zero. With respect to the radial values Fr_R and $Fr_{H\alpha}$, one can see that ‘redder’ SN in general have much lower radial values. Indeed, SNe with colours ‘redder’ than 0.7 exclusively have radial values lower than 0.4 (and lower than 0.3 with respect to $Fr_{H\alpha}$). Meanwhile ‘bluer’ SNe show the full range of radial values, although the very bluest SNe with negative colours appear to have a preference for exploding in the outer regions of their galaxies, as indicated by their large Fr values.

In regions of more intense SF one expects a higher degree of extinction, which is also expected for SNe occurring in more central regions. It is thus probable that the environments where these SNe explode are affecting their colours through line of sight ISM extinction effects, i.e. material in the line of sight reddens the light emitted by the SNe through extinction. A key property of SNe spectra which is assumed to trace the presence and amount of material within the line of sight is narrow sodium (NaD) absorption. The strength of this feature is often used to constrain the amount of host galaxy extinction towards SNe (see e.g. discussion in Poznanski et al. 2012 and Phillips et al. 2013). Hence, within environments where one expects a higher degree of extinction—closer to H II regions or within more central parts of galaxies—one should also see higher absorption due to line of sight material within SNe spectra. The equivalent width (EW) of the unresolved sodium doublet (NaD) was measured for all SNe with available spectra using the method outlined in Förster et al. (2012) and further elaborated in Förster et al. (2013). We then split the samples into those SNe with positive EW measurements, and those without. The results of this analysis are shown in in Figs 19 and 20, where we plot the $H\alpha$ NCR and Fr_R distributions respectively for positive and zero EW measurement sub-samples. The results are striking. With respect to $H\alpha$ NCR, we find that the samples are statistically very different with there being less than a 0.1% chance probability of the two EW distributions being drawn from the same parent population. Indeed only 2 of 20 (10%) events with no EW detection fall on regions of positive $H\alpha$ emission, while this jumps to 24 out of 36 (67%) for SNe with positive EW measurements. Fig. 20 shows that SNe with NaD EW detections are also much more likely to be more central within their galaxies than those without detections, with a $\sim 1\%$ chance of the two distributions being drawn from the same parent population.

The simplest way to explain these results is that ISM material is causing reddening of SNe and also leading to NaD EW detections, where there is more ISM material in the line of sight of SNe when they are found to be coincident with H II regions and/or more centrally. (However, see Pan et al. 2014 who argue that colour diversity is not due to ISM extinction because of the non-correlation with host galaxy extinction as implied from the Balmer decrement.) Circumstellar material in the line of sight could also produce SNe which are both ‘redder’ and are found to more commonly contain NaD absorption. The presence of such material close to the SN could give clues to the true nature of SN Ia progenitors. This would then imply that environmental properties of explosion sites of SNe Ia are determined by a progenitor property and not simply a

chance alignment of a SN with ISM material. A problem with this interpretation is that while it is possible that the radial distribution of SNe Ia could be explained, it is not clear how the CSM material hypothesis can explain that SNe are more often found within H II regions, given the large offset between the lifetimes of H II regions and those of SN Ia progenitors (where above we have suggested the latter must be more than several 100 Myrs). *However*, there are several observational results which further complicate this matter. It was first observed by Sternberg et al. (2011) that absorption of NaD in SNe Ia spectra show an excess of blue-shifted (with respect to host galaxy velocities) profiles. This was further confirmed by Maguire et al. (2013), who also found that those events showing blue-shifted absorption also have stronger absorption components, and were generally found to occur within star-forming galaxies. It is very difficult to explain such blue-shifted profiles through ISM properties. In addition, both NaD absorption properties (Förster et al. 2012, 2013), and SN colours (see e.g. Foley et al. 2011, 2012a; Maeda et al. 2011) have been shown to correlate with many other SN Ia properties, arguing that at least a fraction of their diversity is intrinsic to the SNe themselves (and not solely from ISM effects). We also note that the centralisation of ‘red’ SNe Ia could hint at a metallicity effect. This would then be consistent with the global host properties of our sample when split by SN colour, as presented in Fig. 17.

Returning to Fig. 19 there is another intriguing observations that has yet to be mentioned. Around 25% of SNe Ia *with* NaD absorption detections fall on regions of *zero H α flux*. It is possible that this is simply evidence of significant host galaxy extinction outside of bright H II regions. However, an exciting possibility is that these SNe are those where the NaD features are produced by CSM material. Future environment studies correlating the presence of blue-shifted Na D absorption with host galaxy SF may be particularly revealing in this context.

It is clear that distinguishing between the effects of ISM and CSM extinction for SNe Ia could have profound implications for the discussion of their progenitors. However, as the above shows, such a differentiation is observationally difficult. We have presented further evidence that line of sight material plays a significant role in determining some of the transient features of SNe Ia. Further work will be needed to further elucidate what this means for SN Ia progenitors.

5.4 In the context of previous work

A first study of the immediate environments of SNe Ia was presented by Rigault et al. (2013). These authors measured or set limits on H α emission at the locations of 89 SNe Ia, where they included elliptical host galaxies. Similar to our work, Rigault et al. showed that moderate stretch SNe were found in all types of H α environment. With respect to colour they observed that ‘redder’ SNe were found in higher star-forming environments with a higher flux of H α emission. This is equivalent to our finding using H α NCR pixel statistics (see § 4.1.4 and Fig. 5). Unfortunately we are not in a position to test for environmental effects on Hubble residuals in our sample, as done by those authors, due to the low number of events which could be included in such an analysis. Wang et al. (2013) investigated how spectral velocities of SNe Ia correlate with local environment in terms of radial distributions of SNe (but using normalised distances in place of normalising to flux as done here) and pixel statistics with respect to *u*, *g*, *r*-band light (following the formalism of Fruchter et al. 2006). Similar to our findings, they found that overall the SN Ia population followed the *g* and *r*

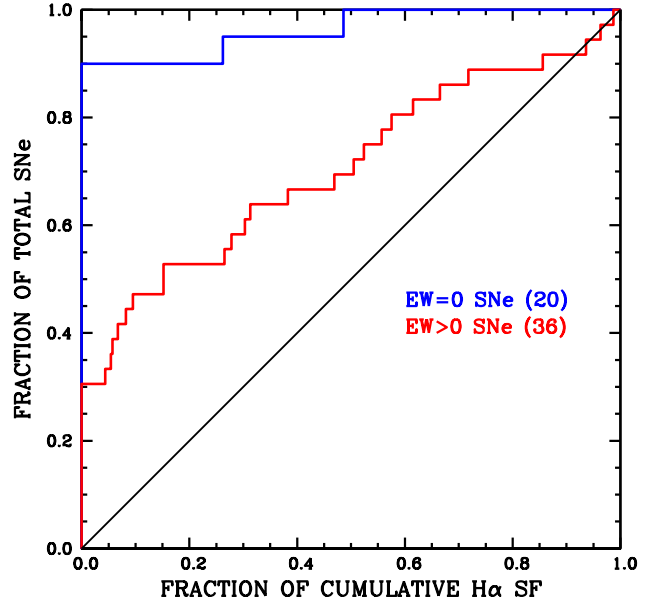


Figure 19. Cumulative H α NCR plot showing distributions of SNe Ia when split into those SNe with and those SNe without NaD absorption in their spectra.

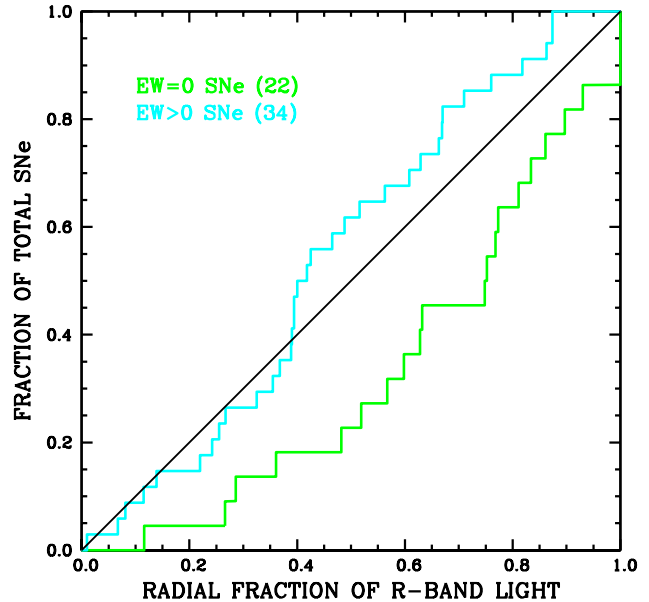


Figure 20. Cumulative plot showing the F_{rR} distributions of SNe Ia when the sample is split into those SNe with and those SNe without NaD absorption in their spectra.

(somewhat equivalent to the analysis presented with respect to the *B* and *R* light distributions) reasonably well, but not the *u*-band light (see their Fig. 3). Wang et al. in particular separated the SN Ia sample into high and low velocity events, claiming for two distinct populations given the differences in environment of the two sub-samples. High velocity events were found to be more centrally within hosts and also to explode on brighter regions (although note the lower significance of this trend in a separate sample as shown

by Pan et al. 2015). While these results are intriguing, we caution on mixing spiral and elliptical hosts when analysing environments. The stellar populations and their distributions are extremely distinct, and it makes more sense to analyse the two samples separately. Here we do not include such an analysis of environments with respect to spectral velocities within exclusively star-forming host galaxies, but such a study in the future may be revealing to confirm the above claims.

The radial distribution of SNe Ia was found to show a deficit in the central regions of spiral galaxies by van den Bergh (1997), as observed above (also see Wang et al. 1997). Galbany et al. (2012) analysed the radial distribution of a sample ~ 200 SNe Ia and concluded that SNe in the more central parts of spiral host galaxies SNe Ia have larger colours (or equivalent parameters) than those SNe in the outer regions, similar to what we have shown. A significant difference between our study and those previously is that we normalise radial positions to flux and not distance, meaning we are analysing where within the radial light-distribution SNe fall.

Overall the results we present are consistent with those previously presented in the literature. SN stretch does not show any significant correlation with local environment in star-forming galaxies, seen through either measurements of the flux at the exact explosion sites, or through analyses of the radial distributions of stretch sub-samples. However, SN colour does seem to show significant correlation with environment.

6 CONCLUSIONS

We have presented statistics on the properties of the environments of SNe Ia within star-forming galaxies. Our main findings are that SNe Ia best trace the B -band light distribution within their galaxies, while they do not trace neither the extreme young populations traced by $H\alpha$ or near-UV emission, nor the evolved populations traced by J - and K -band light. It is found that ‘redder’ SNe are more often found both to be coincident with H II regions and are more centrally concentrated within their host galaxies. In addition, SNe with positive NaD EW measurements are also much more likely to be found in central regions and coincident with bright H II regions. Whether this effect is dominated by ISM or CSM material, or some other progenitor property, remains unresolved. We find a central deficit of SNe Ia with respect to the radial distribution of stellar continuum. Finally, the main conclusions to arise from this investigation are listed below.

□ The SN Ia population best traces the B -band light of their host galaxies. This is in contrast to the $H\alpha$, near-UV, J - and K -band light, where the SNe are inconsistent with being drawn from the underlying populations traced by those bands.

□ ‘Redder’ SNe are found to occur closer to H II regions and also more centrally than their ‘blue’ counterparts. This implies that a significant source of SN colour arises from line of sight material producing extinction and hence reddening effects.

□ While we recover the host galaxy type stretch relation found by numerous previous authors, we find no evidence that stretch is related to environments *within* host galaxies.

□ SNe Ia within star-forming galaxies do not trace the underlying on-going ($H\alpha$) or recent (near-UV) SF. This implies that the dominant population of SNe Ia in star-forming galaxies do not originate from progenitors with delay times of less than a few 100 Myr.

□ Brighter SNe Ia within host galaxies do not follow the spatial distribution of recent SF, implying that even even those SNe Ia associated with a relatively young stellar population do not arise

from extreme ‘prompt’ progenitor channels. This effectively rules out progenitor delay times of less than a few 100 Myr for all but a small minority of events

□ A deficit of SNe Ia is found within the central 20% of the R -band stellar continuum. There is also a suggestion that more SNe Ia per unit SF are produced in the outer regions of galaxies. This observation could be a metallicity effect with lower metallicity populations producing a higher fraction of SNe. Or it could be explained through a progenitor age effect where the central regions of these galaxies have SFHs weighted to older ages, and hence more SNe are produced in the outer regions where younger stellar populations dominate.

ACKNOWLEDGMENTS

We thank the referee Mike Childress for his positive report, and useful suggestions on improving the manuscript. Mark Sullivan, Gaston Folatelli, Giuliano Pignata, Mark Phillips, Lluís Galbany, Mike Bode and Stephen Smartt are thanked for useful discussion. We thank the Carnegie Supernova Project for allowing us to use light-curve fits to unpublished photometry of SN 2009ag. M. H., F. F., and S. G. acknowledge support from the Millennium Institute of Astrophysics (MAS; Programa Iniciativa Científica Milenio del Ministerio de Economía, Fomento y Turismo de Chile, grant IC120009). S. G. thanks CONICYT through FONDECYT grant 3110142. The Liverpool Telescope is operated on the island of La Palma by Liverpool John Moores University in the Spanish Observatorio del Roque de los Muchachos of the Instituto de Astrofísica de Canarias with financial support from the UK Science and Technology Facilities Council. Based on observations made with the Isaac Newton Telescope operated on the island of La Palma by the Isaac Newton Group in the Spanish Observatorio del Roque de los Muchachos of the Instituto de Astrofísica de Canarias, and observations made with the 2.2m MPG/ESO telescope at La Silla, proposal ID: 084.D-0195 and based on observations made with the Nordic Optical Telescope, operated by the Nordic Optical Telescope Scientific Association at the Observatorio del Roque de los Muchachos, La Palma, Spain, of the Instituto de Astrofísica de Canarias This research has made use of the NASA/IPAC Extragalactic Database (NED) which is operated by the Jet Propulsion Laboratory, California Institute of Technology, under contract with the National Aeronautics. Some of the data presented in this paper were obtained from the Mikulski Archive for Space Telescopes (MAST). STScI is operated by the Association of Universities for Research in Astronomy, Inc., under NASA contract NAS5-26555. Support for MAST for non-HST data is provided by the NASA Office of Space Science via grant NNX13AC07G and by other grants and contracts.

REFERENCES

- Altavilla G., et al., 2004, MNRAS, 349, 1344
- Anderson J. P., Habergham S. M., James P. A., Hamuy M., 2012, MNRAS, 424, 1372
- Anderson J. P., James P. A., 2008, MNRAS, 390, 1527
- Anderson J. P., James P. A., 2009, MNRAS, 399, 559
- Aubourg É., Tojeiro R., Jimenez R., Heavens A., Strauss M. A., Spergel D. N., 2008, A&A, 492, 631
- Baade D., et al., 1999, The Messenger, 95, 15

- Bartunov O. S., Tsvetkov D. Y., Filimonova I. V., 1994, *PASP*, 106, 1276
- Biscardi I., et al., 2012, *A&A*, 537, A57
- Bloom J. S., et al., 2012, *ApJ Let.*, 744, L17
- Branch D., Miller D. L., 1993, *ApJ Let.*, 405, L5
- Bruzual G., Charlot S., 2003, *MNRAS*, 344, 1000
- Childress M., et al., 2013, *ApJ*, 770, 108
- Childress M. J., Wolf C., Zahid H. J., 2014, *MNRAS*, 445, 1898
- Conley A., et al., 2008, *ApJ*, 681, 482
- Contreras C., et al., 2010, *AJ*, 139, 519
- D'Andrea C. B., et al., 2011, *ApJ*, 743, 172
- Elias-Rosa N., et al., 2006, *MNRAS*, 369, 1880
- Foley R. J., et al., 2012a, *ApJ*, 752, 101
- Foley R. J., et al., 2012b, *ApJ*, 744, 38
- Foley R. J., Sanders N. E., Kirshner R. P., 2011, *ApJ*, 742, 89
- Ford C. H., et al., 1993, *AJ*, 106, 1101
- Förster F., et al., 2012, *ApJ Let.*, 754, L21
- Förster F., González-Gaitán S., Folatelli G., Morrell N., 2013, *ApJ*, 772, 19
- Förster F., Schawinski K., 2008, *MNRAS*, 388, L74
- Förster F., Wolf C., Podsiadlowski P., Han Z., 2006, *MNRAS*, 368, 1893
- Fruchter A. S., et al., 2006, *Nature*, 441, 463
- Galbany L., et al., 2012, *ApJ*, 755, 125
- Galbany L., et al., 2014, *A&A*, 572, A38
- Gallagher J. S., Garnavich P. M., Caldwell N., Kirshner R. P., Jha S. W., Li W., Ganeshalingam M., Filippenko A. V., 2008, *ApJ*, 685, 752
- Ganeshalingam M., et al., 2010, *ApJS*, 190, 418
- Garnavich P. M., et al., 2004, *ApJ*, 613, 1120
- Gogarten S. M., et al., 2009, *ApJ*, 691, 115
- Gupta R. R., et al., 2011, *ApJ*, 740, 92
- Habergham S. M., Anderson J. P., James P. A., 2010, *ApJ*, 717, 342
- Habergham S. M., Anderson J. P., James P. A., Lyman J. D., 2014, *MNRAS*, 441, 2230
- Habergham S. M., James P. A., Anderson J. P., 2012, *MNRAS*, 424, 2841
- Hachisu I., Kato M., Saio H., Nomoto K., 2012, *ApJ*, 744, 69
- Hakobyan A. A., et al., 2014, *MNRAS*, 444, 2428
- Hamuy M., et al., 1996, *AJ*, 112, 2408
- Hamuy M., Phillips M. M., Suntzeff N. B., Schommer R. A., Maza J., Aviles R., 1996a, *AJ*, 112, 2391
- Hamuy M., Phillips M. M., Suntzeff N. B., Schommer R. A., Maza J., Aviles R., 1996b, *AJ*, 112, 2398
- Hamuy M., Trager S. C., Pinto P. A., Phillips M. M., Schommer R. A., Ivanov V., Suntzeff N. B., 2000, *AJ*, 120, 1479
- Hayden B. T., Gupta R. R., Garnavich P. M., Mannucci F., Nichol R. C., Sako M., 2013, *ApJ*, 764, 191
- Henry R. B. C., Worthey G., 1999, *PASP*, 111, 919
- Hicken M., et al., 2009, *ApJ*, 700, 331
- Hicken M., et al., 2012, *ApJS*, 200, 12
- Howell D. A., et al., 2009, *ApJ*, 691, 661
- Iben Jr. I., Tutukov A. V., 1984, *ApJS*, 54, 335
- Ivanov V. D., Hamuy M., Pinto P. A., 2000, *ApJ*, 542, 588
- James P. A., Anderson J. P., 2006, *A&A*, 453, 57
- James P. A., et al., 2004, *A&A*, 414, 23
- Jha S., et al., 2006, *AJ*, 131, 527
- Johansson J., et al., 2013, *MNRAS*, 435, 1680
- Kangas T., Mattila S., Kankare E., Kotilainen J. K., Väisänen P., Greimel R., Takalo A., 2013, *MNRAS*, 436, 3464
- Kelly P. L., Filippenko A. V., Burke D. L., Hicken M., Ganeshalingam M., Zheng W., 2014, *ArXiv e-prints*, 1410.0961
- Kelly P. L., Hicken M., Burke D. L., Mandel K. S., Kirshner R. P., 2010, *ApJ*, 715, 743
- Kelly P. L., Kirshner R. P., 2012, *ApJ*, 759, 107
- Kelly P. L., Kirshner R. P., Pahre M., 2008, *ApJ*, 687, 1201
- Kennicutt Jr. R. C., 1998, *ARA&A*, 36, 189
- Kistler M. D., Stanek K. Z., Kochanek C. S., Prieto J. L., Thompson T. A., 2013, *ApJ*, 770, 88
- Kobayashi C., Nomoto K., 2009, *ApJ*, 707, 1466
- Kobayashi C., Tsujimoto T., Nomoto K., Hachisu I., Kato M., 1998, *ApJ Let.*, 503, L155
- Krisciunas K., et al., 2000, *ApJ*, 539, 658
- Krisciunas K., et al., 2004, *AJ*, 128, 3034
- Krisciunas K., et al., 2006, *AJ*, 131, 1639
- Lair J. C., Leising M. D., Milne P. A., Williams G. G., 2006, *AJ*, 132, 2024
- Lampeitl H., et al., 2010, *ApJ*, 722, 566
- Leonard D. C., Li W., Filippenko A. V., Foley R. J., Chornock R., 2005, *ApJ*, 632, 450
- Li W., et al., 2011, *MNRAS*, 412, 1473
- Lira P., et al., 1998, *AJ*, 115, 234
- Maeda K., et al., 2011, *MNRAS*, 413, 3075
- Maguire K., et al., 2013, *MNRAS*, 436, 222
- Mannucci F., Della Valle M., Panagia N., 2006, *MNRAS*, 370, 773
- Mannucci F., Della Valle M., Panagia N., Cappellaro E., Cresci G., Maiolino R., Petrosian A., Turatto M., 2005, *A&A*, 433, 807
- Maoz D., Mannucci F., Brandt T. D., 2012, *MNRAS*, 426, 3282
- Maoz D., Mannucci F., Li W., Filippenko A. V., Della Valle M., Panagia N., 2011, *MNRAS*, 412, 1508
- Maoz D., Mannucci F., Nelemans G., 2014, *ARA&A*, 52, 107
- Maraston C., 2005, *MNRAS*, 362, 799
- Matteucci F., Panagia N., Pipino A., Mannucci F., Recchi S., Della Valle M., 2006, *MNRAS*, 372, 265
- Meikle W. P. S., et al., 1996, *MNRAS*, 281, 263
- Modjaz M., Kewley L., Kirshner R. P., Stanek K. Z., Challis P., Garnavich P. M., Greene J. E., Kelly P. L., Prieto J. L., 2008, *AJ*, 135, 1136
- Neill J. D., et al., 2009, *ApJ*, 707, 1449
- Nomoto K., 1982, *ApJ*, 257, 780
- Nugent P. E., et al., 2011, *Nature*, 480, 344
- Pakmor R., Kromer M., Taubenberger S., Sim S. A., Röpke F. K., Hillebrandt W., 2012, *ApJ Let.*, 747, L10
- Pan Y.-C., et al., 2014, *MNRAS*, 438, 1391
- Pan Y.-C., et al., 2015, *MNRAS*, 446, 354
- Patat F., et al., 1996, *MNRAS*, 278, 111
- Perlmutter S., et al., 1997, *ApJ*, 483, 565
- Perlmutter S., et al., 1999, *ApJ*, 517, 565
- Phillips M. M., 1993, *ApJ Let.*, 413, L105
- Phillips M. M., et al., 1987, *PASP*, 99, 592
- Phillips M. M., et al., 2013, *ApJ*, 779, 38
- Pierce M. J., Jacoby G. H., 1995, *AJ*, 110, 2885
- Pietrinferni A., Cassisi S., Salaris M., Castelli F., 2004, *ApJ*, 612, 168
- Pignata G., et al., 2004, *MNRAS*, 355, 178
- Poznanski D., Prochaska J. X., Bloom J. S., 2012, *MNRAS*, 426, 1465
- Prieto J. L., Stanek K. Z., Beacom J. F., 2008, *ApJ*, 673, 999
- Quimby R. M., Yuan F., Akerlof C., Wheeler J. C., Warren M. S., 2012, *AJ*, 144, 177

- Raskin C., Scannapieco E., Rhoads J., Della Valle M., 2009, *ApJ*, 707, 74
- Riess A. G., et al., 1998, *AJ*, 116, 1009
- Riess A. G., et al., 1999, *AJ*, 117, 707
- Riess A. G., et al., 2005, *ApJ*, 627, 579
- Riess A. G., Press W. H., Kirshner R. P., 1996, *ApJ*, 473, 88
- Rigault M., et al., 2013, *A&A*, 560, A66
- Sandage A., Tammann G. A., 1993, *ApJ*, 415, 1
- Scalzo R., et al., 2014, *MNRAS*, 440, 1498
- Scannapieco E., Bildsten L., 2005, *ApJ Let.*, 629, L85
- Schawinski K., Thomas D., Sarzi M., Maraston C., Kaviraj S., Joo S.-J., Yi S. K., Silk J., 2007, *MNRAS*, 382, 1415
- Smith M., Nichol R. C., Dilday B., Marriner J., Kessler R., Bassett B., Cinabro D., Frieman J., Garnavich P., Jha S. W., Lampeitl H., Sako M., Schneider D. P., Sollerman J., 2012, *ApJ*, 755, 61
- Steele I. A., et al., 2004, in Oschmann Jr. J. M., ed., *Ground-based Telescopes*. Edited by Oschmann, Jacobus M., Jr. Proceedings of the SPIE, Volume 5489, pp. 679-692 (2004). Vol. 5489 of Presented at the Society of Photo-Optical Instrumentation Engineers (SPIE) Conference, The Liverpool Telescope: performance and first results. pp 679–692
- Sternberg A., et al., 2011, *Science*, 333, 856
- Stritzinger M. D., et al., 2011, *AJ*, 142, 156
- Strolger L.-G., et al., 2004, *ApJ*, 613, 200
- Sullivan M., et al., 2006, *ApJ*, 648, 868
- Sullivan M., et al., 2010, *MNRAS*, 406, 782
- Suntzeff N. B., et al., 1999, *AJ*, 117, 1175
- Tsvetkov D. Y., 2006, *Peremennye Zvezdy*, 26, 3
- Tsvetkov D. Y., Elenin L., 2010, *Peremennye Zvezdy*, 30, 2
- Valentini G., et al., 2003, *ApJ*, 595, 779
- van den Bergh S., 1997, *AJ*, 113, 197
- van den Bergh S., Li W., Filippenko A. V., 2002, *PASP*, 114, 820
- Wang B., Han Z., 2012, *NewAR*, 56, 122
- Wang L., Höflich P., Wheeler J. C., 1997, *ApJ Let.*, 483, L29
- Wang X., et al., 2009, *ApJ*, 697, 380
- Wang X., Wang L., Filippenko A. V., Zhang T., Zhao X., 2013, *Science*, 340, 170
- Wells L. A., et al., 1994, *AJ*, 108, 2233
- Whelan J., Iben I. J., 1973, *ApJ*, 186, 1007
- Worthey G., 1994, *ApJS*, 95, 107
- Zheng W., et al., 2013, *ApJ Let.*, 778, L15

APPENDIX A: SN ENVIRONMENT STATISTICS

Table A1. SNe environment statistical analyses values. In the first column the SN name is listed. This is followed by the NCR values derived from $H\alpha$, near-UV, B -band, R -band, J -band and K -band in columns 2, 3, 4, 5, 6, and 7 respectively. In columns 8 and 9 the Fr_R and $Fr_{H\alpha}$ are listed.

| SN | NCR $_{H\alpha}$ | NCR $_{nUV}$ | NCR $_B$ | NCR $_R$ | NCR $_J$ | NCR $_K$ | Fr_R | $Fr_{H\alpha}$ |
|--------|------------------|--------------|----------|----------|----------|----------|--------|----------------|
| 1937C | 0.555 | 0.240 | ... | ... | ... | ... | 0.272 | 0.340 |
| 1954B | 0.466 | 0.537 | 0.629 | 0.719 | 0.440 | 0.000 | 0.253 | 0.137 |
| 1957A | 0.000 | 0.572 | ... | 0.076 | ... | ... | 0.797 | 0.831 |
| 1963I | 0.317 | 0.319 | 0.792 | 0.557 | 0.625 | 0.808 | 0.111 | 0.068 |
| 1963J | 0.000 | ... | 0.721 | 0.346 | 0.466 | 0.000 | 0.307 | 0.126 |
| 1968E | 0.277 | 0.599 | 0.567 | 0.503 | 0.485 | 0.471 | 0.560 | 0.577 |
| 1968I | 0.000 | 0.000 | 0.639 | 0.822 | 0.769 | 0.774 | 0.137 | 0.063 |
| 1969C | 0.297 | ... | ... | 0.709 | ... | ... | 0.300 | 0.178 |
| 1971G | 0.030 | 0.038 | ... | 0.011 | 0.422 | 0.000 | 0.794 | 0.956 |
| 1972H | 0.000 | 0.281 | 0.498 | 0.344 | 0.253 | 0.016 | 0.646 | 0.750 |
| 1974G | 0.000 | 0.367 | 0.000 | 0.336 | 0.137 | 0.032 | 0.772 | 0.816 |
| 1975A | 0.000 | 0.000 | ... | ... | ... | ... | 0.722 | 0.672 |
| 1979B | 0.000 | ... | 0.288 | 0.725 | 0.000 | 0.000 | 0.784 | 0.670 |
| 1981B | 0.000 | ... | ... | 0.158 | ... | ... | 0.731 | 0.747 |
| 1982B | 0.000 | 0.484 | 0.560 | 0.367 | 0.453 | 0.278 | 0.507 | 0.572 |
| 1983U | 0.000 | ... | ... | ... | ... | ... | 0.365 | 0.735 |
| 1986A | 0.249 | 0.038 | 0.735 | 0.682 | 0.397 | 0.000 | 0.433 | 0.437 |
| 1986G | 0.069 | ... | ... | ... | ... | ... | ... | ... |
| 1987D | 0.000 | 0.356 | ... | 0.425 | ... | ... | 0.485 | 0.963 |
| 1987O | 0.000 | 0.000 | ... | ... | ... | ... | 0.672 | 0.755 |
| 1989A | 0.000 | 0.238 | ... | 0.160 | 0.000 | 0.000 | 0.674 | 0.726 |
| 1989B | 0.544 | ... | ... | 0.732 | ... | ... | 0.276 | 0.216 |
| 1990N | 0.000 | 0.000 | ... | 0.089 | ... | ... | 0.869 | 0.872 |
| 1991ak | 0.000 | 0.652 | 0.454 | 0.363 | 0.301 | 0.000 | 0.645 | 0.655 |
| 1991T | 0.000 | 0.000 | 0.355 | 0.072 | 0.126 | 0.253 | 0.578 | 0.395 |
| 1992bc | 0.000 | 0.000 | ... | 0.000 | ... | ... | 0.898 | 0.566 |
| 1992G | 0.343 | 0.539 | 0.757 | 0.761 | 0.707 | 0.630 | 0.335 | 0.351 |
| 1992K | 0.395 | 0.663 | ... | ... | ... | ... | 0.214 | 0.156 |
| 1994ae | 0.000 | 0.026 | 0.261 | 0.205 | 0.000 | 0.099 | 0.748 | 0.720 |
| 1994S | 0.082 | 0.000 | ... | 0.278 | ... | ... | 0.670 | 0.876 |
| 1995al | 0.054 | 0.300 | 0.333 | 0.328 | 0.330 | 0.234 | 0.488 | 0.557 |
| 1995D | 0.000 | 0.000 | 0.000 | 0.000 | 0.000 | 0.000 | 0.930 | 0.975 |
| 1995E | 0.000 | 0.345 | 0.881 | 0.862 | 0.846 | 0.737 | 0.394 | 0.284 |
| 1996ai | 0.615 | 0.232 | 0.810 | 0.801 | 0.661 | 0.661 | 0.325 | 0.292 |
| 1996Z | 0.000 | ... | ... | 0.000 | ... | ... | 0.768 | 0.748 |
| 1997bp | 0.095 | 0.213 | ... | 0.266 | ... | ... | 0.710 | 0.862 |
| 1997bq | 0.000 | 0.096 | 0.184 | 0.170 | 0.000 | 0.000 | 0.818 | 0.932 |
| 1997do | 0.486 | 0.967 | 0.940 | 0.905 | 0.749 | 0.736 | 0.116 | 0.095 |
| 1997dt | 0.524 | ... | ... | 0.916 | ... | ... | 0.355 | 0.281 |
| 1997Y | 0.303 | ... | 0.371 | 0.810 | 0.633 | 0.467 | 0.139 | 0.259 |
| 1998aq | 0.262 | ... | 0.460 | 0.426 | 0.313 | 0.083 | 0.628 | 0.814 |
| 1998bu | 0.000 | 0.798 | ... | 0.424 | ... | ... | 0.519 | 0.034 |
| 1998D | 0.000 | 0.000 | 0.337 | 0.178 | 0.208 | 0.164 | 0.608 | 0.795 |
| 1998dh | 0.044 | ... | ... | 0.339 | ... | ... | 0.465 | 0.449 |
| 1998eb | 0.000 | 0.175 | ... | ... | ... | ... | 0.516 | 0.554 |
| 1999aa | 0.000 | 0.473 | 0.638 | 0.600 | 0.398 | 0.513 | 0.482 | 0.270 |
| 1999bh | 0.856 | ... | 0.599 | 0.446 | 0.348 | 0.450 | 0.418 | 0.232 |
| 1999bv | 0.000 | ... | ... | 0.000 | ... | ... | 0.834 | 0.618 |
| 1999by | 0.000 | 0.534 | ... | 0.160 | ... | ... | 0.752 | 0.789 |
| 1999cl | 0.152 | 0.264 | ... | ... | ... | ... | ... | ... |
| 1999cp | 0.000 | 0.000 | 0.000 | 0.073 | 0.000 | 0.000 | 0.811 | 0.791 |
| 1999gd | 0.000 | 0.000 | 0.359 | 0.346 | 0.186 | 0.000 | 0.874 | 0.929 |
| 2000ce | 0.505 | ... | 0.500 | 0.392 | 0.000 | 0.135 | 0.563 | 0.507 |
| 2000E | 0.718 | 0.000 | ... | ... | ... | ... | 0.368 | 0.279 |
| 2001ay | ... | ... | ... | ... | ... | ... | 0.638 | 0.384 |
| 2001bg | 0.000 | 0.145 | 0.207 | 0.212 | 0.000 | 0.000 | 0.760 | 0.902 |
| 2001cz | 0.000 | 0.102 | ... | 0.363 | ... | ... | 0.461 | 0.346 |
| 2001E | 0.265 | 0.435 | 0.503 | 0.477 | 0.283 | 0.133 | 0.663 | 0.384 |
| 2001eg | 0.000 | 0.000 | 0.225 | 0.265 | 0.000 | 0.606 | 0.605 | 0.774 |
| 2002au | 0.096 | 0.825 | 0.481 | 0.374 | 0.344 | 0.000 | 0.764 | 0.864 |
| 2002bs | 0.963 | 0.988 | 0.993 | 0.991 | 0.956 | 0.934 | 0.010 | 0.009 |
| 2002cr | 0.000 | 0.066 | 0.000 | 0.052 | 0.000 | 0.000 | 0.874 | 0.936 |
| 2002er | 0.278 | 0.000 | ... | 0.564 | 0.180 | ... | 0.394 | 0.678 |

Table A1. Continued...

| SN | NCR _{Hα} | NCR _{nUVV} | NCR _B | NCR _R | NCR _J | NCR _K | Fr _R | Fr _{Hα} |
|--------|-------------------------------------|---------------------|------------------|------------------|------------------|------------------|-----------------|------------------------------------|
| 2002fk | 0.000 | 0.636 | ... | ... | ... | ... | 0.266 | 0.095 |
| 2003cg | 0.557 | 0.369 | ... | 0.693 | ... | ... | 0.242 | 0.142 |
| 2003cp | 0.000 | ... | 0.606 | 0.509 | 0.023 | 0.000 | 0.494 | 0.605 |
| 2003du | 0.000 | 0.432 | 0.670 | 0.000 | 0.000 | ... | 0.286 | 0.205 |
| 2004bc | 0.987 | 0.821 | ... | 0.966 | ... | ... | 0.389 | 0.189 |
| 2004bd | 0.665 | 0.214 | 0.865 | 0.862 | 0.759 | 0.769 | 0.115 | 0.434 |
| 2005A | 0.000 | 0.398 | ... | 0.506 | ... | ... | 0.255 | 0.136 |
| 2005am | 0.000 | 0.000 | 0.330 | 0.000 | 0.265 | 0.255 | 0.632 | 0.670 |
| 2005bc | 0.313 | ... | 0.770 | 0.751 | 0.716 | 0.725 | 0.267 | 0.386 |
| 2005bo | 0.152 | 0.653 | 0.387 | 0.456 | 0.420 | 0.376 | 0.390 | 0.405 |
| 2005cf | 0.000 | 0.000 | ... | ... | ... | ... | 1.000 | 1.000 |
| 2005el | 0.000 | ... | ... | 0.000 | ... | ... | 0.567 | 0.870 |
| 2005F | ... | ... | ... | ... | ... | ... | 0.975 | 1.000 |
| 2005G | ... | ... | ... | ... | ... | ... | 0.773 | 0.656 |
| 2005ke | 0.000 | 0.069 | ... | ... | ... | ... | 0.861 | 0.815 |
| 2005M | ... | ... | ... | ... | ... | ... | 0.897 | 0.940 |
| 2005W | 0.000 | 0.000 | ... | ... | ... | ... | 0.669 | 0.562 |
| 2006ax | 0.057 | 0.000 | ... | 0.057 | ... | ... | 0.863 | 0.990 |
| 2006ce | 0.000 | 0.000 | ... | 0.090 | ... | ... | 0.850 | 0.887 |
| 2006D | 0.000 | 0.000 | ... | 0.366 | ... | ... | 0.598 | 1.000 |
| 2006mq | 0.000 | ... | ... | ... | ... | ... | ... | ... |
| 2006N | 0.000 | 0.756 | 0.560 | 0.591 | 0.451 | 0.592 | 0.400 | 0.534 |
| 2006ou | 0.000 | ... | ... | 0.562 | ... | ... | 0.220 | 0.282 |
| 2006X | 0.067 | 0.201 | ... | ... | ... | ... | ... | ... |
| 2007af | 0.469 | 0.306 | ... | 0.372 | ... | ... | 0.629 | 0.558 |
| 2007bm | 0.383 | 0.449 | ... | 0.910 | ... | ... | 0.067 | 0.034 |
| 2007N | 0.000 | 0.000 | ... | 0.429 | ... | ... | 0.361 | 0.282 |
| 2007S | 0.575 | 0.641 | ... | 0.526 | ... | ... | 0.425 | 0.405 |
| 2007sr | 0.000 | ... | ... | ... | ... | ... | 1.000 | 1.000 |
| 2008bi | 0.936 | 0.722 | ... | 0.906 | ... | ... | 0.081 | 0.029 |
| 2008fv | 0.261 | 0.631 | 0.373 | 0.478 | 0.318 | 0.152 | 0.564 | 0.515 |
| 2009ag | 0.000 | ... | ... | ... | ... | ... | 1.000 | 1.000 |
| 2009ds | 0.169 | 0.896 | 0.771 | 0.767 | 0.722 | 0.909 | 0.227 | 0.124 |
| 2009ig | 0.000 | ... | ... | 0.480 | ... | ... | 0.511 | 0.013 |
| 2010eb | 0.000 | 0.000 | ... | 0.000 | ... | ... | 1.000 | 1.000 |
| 2011ao | 0.000 | 0.301 | ... | 0.545 | ... | ... | 0.398 | 0.379 |
| 2011B | ... | ... | ... | ... | ... | ... | 0.247 | 1.000 |
| 2011dm | 0.000 | ... | ... | ... | ... | ... | 1.000 | 1.000 |
| 2011dx | 0.000 | 0.209 | ... | 0.218 | ... | ... | 0.755 | 0.706 |
| 2011ek | 0.000 | 0.000 | ... | 0.000 | ... | ... | 1.000 | 1.000 |